CZECH TECHNICAL UNIVERSITY IN PRAGUE

FACULTY OF BIOMEDICAL ENGINEERING
Department of biomedical technology

Simulátor elektromagnetického pole FDTD pro studium algoritmů plánování léčby

FDTD-based electromagnetic field simulator for studying treatment planning algorithms

Bachelor's Thesis

Study programme: Biomedical and Clinical Technology
Study branch: Biomedical Technician

Supervisor: prof. Dr.-Ing. Jan Vrba, M.Sc.

Ksenia Kulakova

Kladno 2022

BACHELOR'S THESIS ASSIGNMENT

CTU CZECH TECHNICAL UNIVERSITY IN PRAGUE

I. PERSONAL AND STUDY DETAILS

Student's name:	**Kulakova Ksenia**	Personal ID number: **491299**
Faculty:	**Faculty of Biomedical Engineering**	
Department:	**Department of Biomedical Technology**	
Study program:	**Biomedical and Clinical Technology**	
Branch of study:	**Biomedical Technician**	

II. BACHELOR'S THESIS DETAILS

Bachelor's thesis title in English:

FDTD-based electromagnetic field simulator for studying treatment planning algorithms

Bachelor's thesis title in Czech:

Simulátor elektromagnetického pole FDTD pro studium algoritmů plánování léčby

Guidelines:

In MATLAB, implement a) 2D FDTD-based numerical simulator of electromagnetic fields and b) model of a 4 channel hyperthermia applicator, water bolus, and of a 2D anatomically and dielectrically realistic model of the pelvic area. Create a corresponding numerical model in COMSOL Multiphysics and compare calculated electromagnetic fields from both simulators. Implement four different beam steering strategies: 1) THQ driven global optimization, 2) Generalized Eigenvalue Approach, 3) Time-Reversal, and 4) Target Centre Point (TCP) steering. Implement in clinics used parameters for evaluation of treatment planning quality TC25 and TC50. For 10 different target locations evaluate the treatment planning quality for all four beam steering strategies.

Bibliography / sources:

[1] Dennis M. Sullivan, Electromagnetic Simulation Using the FDTD Method, ed. 1st, IEEE Press, 2000, ISBN 0-7803-4747-1
[2] John G. Webster, Encyclopedia of Medical Devices and Instrumentation, ed. 6, Wiley, 2006, ISBN 978-0-471-26358-6
[3] Kok, H. P., Wust, P., Stauffer, P. R., Bardati, F., van Rhoon, G. C., & Crezee, J. , Current state of the art of regional hyperthermia treatment planning: a review, Radiation oncology , ročník 10, číslo 196, 2015, 14 s., https://doi.org/10.1186/s13014-015-0503-8

Name of bachelor's thesis supervisor:

prof. Dr.-Ing. Jan Vrba, M.Sc.

Name of bachelor's thesis consultant:

Ing. Tomáš Dřížďal, Ph.D.

Date of bachelor's thesis assignment: **14.02.2022**
Assignment valid until: **22.09.2023**

doc. Ing. Martin Rožánek, Ph.D.	prof. MUDr. Jozef Rosina, Ph.D., MBA
Head of department	Dean

Declaration

I hereby declare that I have completed this bachelor thesis with the topic "FDTD-based electromagnetic field simulator for studying treatment planning algorithms" independently, and that I have attached an exhaustive list of citations of the employed sources to the Bachelor Thesis.

I do not have a compelling reason against the use of the bachelor thesis within the meaning of Section 60 of the Act No.121 / 2000 Coll., on copyright, rights related to copyright and amending some laws (Copyright Act).

In Kladno 11.5.2022

Ksenia Kulakova

Acknowledgements

ABSTRAKT

Simulátor elektromagnetického pole FDTD pro studium algoritmů plánování léčby

Rakovina pánevní oblasti je jednou z nejčastějších příčin úmrtí na rakovinu, a proto vyžaduje zvláštní pozornost. Nedávno provedené studie ukázaly, že mikrovlnná hypertermie představuje neinvazivní metodu, kterou lze účinně integrovat do procesů léčby rakoviny a zvýšit celkovou účinnost léčby. Hlavním cílem této práce bylo, jako příspěvek k výzkumu v této oblasti, vyvinout v prostředí MATLAB numerický simulátor elektromagnetického pole v anatomicky a dielektricky realistickém modelu oblasti léčené mikrovlnnou hypertermií založený na metodě FDTD a využít jej pro studium dostupných algoritmy plánování léčby. Metoda FDTD byla zvolena pro její srozumitelnost, vhodnost pro uvažovaný problém a kompatibilitu s prostředím MATLAB. Dalším důvodem pro vývoj vlastního simulátoru elektromagnetického pole v prostředí MATLAB je již v tomto prostředí implementovaný software pro plánování léčby a řízení laboratorního prototypu regionálního mikrovlnného hypertermického systému vyvíjeného na FBMI ČVUT. Elektromagnetická pole vypočtená zde vyvinutým simulátorem vykazují dobrou shodu s elektromagnetickými poli vypočtenými osvědčeným komerčním simulátorem COMSOL Multiphysics. Vyvinutý model a simulátor je vhodný pro kvalitativní i kvantitativní hodnocení algoritmů plánování léčby. Dále byly implementovány čtyři různé strategie plánování léčby: 1) globální optimalizace řízená parametrem THQ, 2) zobecněný přístup vlastních hodnot, 3) metoda time-reversal a 4) metoda cílového středového bodu (TCP). Pro jeden anatomicky a dielektricky realistický model pacienta, deset různých modelů cílů léčby a čtyř výše uvedené strategie byla pomocí v klinice používaných parametrů TC25, TC50 a THQ vyhodnocena a vzájemně porovnána kvalita plánování léčby.

Klíčová slova

Elektromagnetické pole, FDTD, MATLAB, numerický simulátor, mikrovlnná hypertermie, algoritmy plánování léčby.

ABSTRACT

FDTD-based electromagnetic field simulator for studying treatment planning algorithms

Pelvic cancer is one of the most common causes of deaths due to cancer, and, therefore, requires special attention. Recent studies have shown that microwave hyperthermia is a promising non-invasive approach that can effectively be integrated into cancer treatment processes. As a contribution to research in this field, the main aim of this thesis was to develop a numerical simulator of electromagnetic field in an anatomically and dielectrically realistic model of area treated with microwave hyperthermia in MATLAB environment using the FDTD method and use it for studying available treatment planning algorithms. The FDTD method was chosen due to its clarity, suitability for the problem raised in this thesis, and compatibility with MATLAB. Another reason for the development of own electromagnetic field simulator in MATLAB environment is that the laboratory prototype of the software for treatment planning and for the control of regional microwave hyperthermia developed at the FBME CTU is being implemented in MATLAB. The electromagnetic field calculated by the developed FDTD simulator shows a good agreement with the electromagnetic field calculated by the well-proven commercial simulator COMSOL Multiphysics. The developed model and simulator are well-suited for both qualitative and quantitative assessment of the performance of treatment planning algorithms in various scenarios. In addition, four different treatment planning strategies were implemented: 1) global optimization controlled by the THQ parameter, 2) generalized eigenvalue approach, 3) time-reversal, and 4) target center point (TCP) method. For one anatomically and dielectrically realistic patient model, ten different treatment target models, and the four strategies mentioned above, the quality of treatment planning was evaluated and compared with the parameters used in clinics, namely TC25, TC50 and THQ.

Key words

Electromagnetic field, FDTD, MATLAB, numerical simulator, microwave hyperthermia, treatment planning algorithms.

Contents

List of Symbols and Abbreviations

List of Symbols

Symbol	Unit	Meaning
pO_2	Pa	Partial pressure of oxygen
RF	Hz	Radiofrequency
SAR	$\text{W} \cdot \text{kg}^{-1}$	Specific Absorption Rate
E	$\text{V} \cdot \text{m}^{-1}$	Electric field intensity
H	$\text{A} \cdot \text{m}^{-1}$	Magnetic field intensity
t	s	Time
ε_0	$\text{F} \cdot \text{m}^{-1}$	Permittivity of vacuum
μ_0	$\text{H} \cdot \text{m}^{-1}$	Permeability of vacuum
n	-	Sample time instant
k	-	Sample spatial point
ω	$\text{rad} \cdot \text{s}^{-1}$	Angular frequency
$\epsilon_{r\infty}$	-	Relative permittivity at high frequencies
$\Delta\epsilon_{ri\infty}$	-	Magnitude of the dispersion
τ	s	Relaxation time
α	-	Parameter related to the broadening of the dispersion
σ	$\text{S} \cdot \text{m}^{-1}$	Static ionic (electrical) conductivity of the tissue
ϵ_0	$\text{F} \cdot \text{m}^{-1}$	Vacuum permittivity
$\text{E}_{z,total}$	$\text{V} \cdot \text{m}^{-1}$	Total phasor
$\text{E}_{z,i}$	$\text{V} \cdot \text{m}^{-1}$	Individual phasor for each source
A_i	$\text{V} \cdot \text{m}^{-1}$	Amplitude value of the pulse from the respective source
ϕ_i	rad	Phase of the pulse from each antenna
c	$\text{m} \cdot \text{s}^{-1}$	Speed of light in vacuum
ε_r	-	Relative permittivity of the tissue
r_0	m	Position of a point source within the tumor
r	m	Position of a point source at a specific time instant
r_1	m	Position of a point source on the cavity surface
μ	$\text{H} \cdot \text{m}^{-1}$	Permeability of the environment in which the electromagnetic wave propagates
T	s	Time after which the recorded field vanishes

List of Abbreviations

Abbreviation	Meaning
ABC	Absorbing Boundary Condition
CPU	Central Processing Unit
CT	Computed Tomography
DIVA	Discrete Vasculature
DNA	Deoxyribonucleic acid
E-field	Electric field
EM	Electromagnetic
FDTD	Finite-Difference-Time-Domain
FE	Finite Element
FIT	Finite Integration Technique
GPU	Graphics Processing Unit
H-field	Magnetic field
HIFU	High-intensity Focused Ultrasound
HT	Hyperthermia
HTP	Hyperthermia Treatment Planning
MR	Magnetic Resonance
MRI	Magnetic Resonance Imaging
MW EM	Microwave Electromagnetic
NIT	Non-invasive Thermometry
pH	Scale used to specify the acidity or basicity of an aqueous solution
PSO	Particle Swarm Optimisation
RT	Radiotherapy
THQ	Target to Hot-Spot Quotient
3-D	Three-Dimensional
VSIE	Volume Surface Integral Equation
WF-CGFFT	Weak Form of the Conjugate Gradient Fast Fourier Transform

List of Tables

List of Figures

1 Introduction

In today's world, the rapid and progressive development of medicine lets humanity successfully and effectively treat numerous diseases, either with the use of relatively simple therapy or a much more complex and sophisticated approach. As every science, medicine also faces challenges and the necessity to deal with questions that still do not have a definite answer. One of them is finding an effective way to treat cancer. In 2020, almost 10 million cancer deaths occurred worldwide, with lung cancer (11.4 % out of the total death cases) being the most common cause of mortality in cancer patients [7]. Nowadays cancer presents a great threat to the world's population including all age groups, genders and nationalities. This can be seen if a closer look is taken at statistics provided for the year 2017, with cancer being the second major cause of death following cardiovascular diseases (see Figure 1.1) [1].

Number of deaths by cause, World, 2017

Cause	Number
Cardiovascular diseases	17.79 million
Cancers	9.56 million
Respiratory diseases	3.91 million
Lower respiratory infections	2.56 million
Dementia	2.51 million
Digestive diseases	2.38 million
Neonatal disorders	1.78 million
Diarrheal diseases	1.57 million
Diabetes	1.37 million
Liver diseases	1.32 million
Road injuries	1.24 million
Kidney disease	1.23 million
Tuberculosis	1.18 million
HIV/AIDS	954,491.75
Suicide	793,823.47
Malaria	619,826.63
Homicide	405,346.24
Parkinson disease	340,639.17
Drowning	295,210.43
Meningitis	288,021.11
Nutritional deficiencies	269,996.92
Protein-energy malnutrition	231,770.99
Maternal disorders	193,639.31
Alcohol use disorders	184,934.24
Drug use disorders	166,612.55
Conflict	129,720.15
Hepatitis	126,390.59
Fire	120,631.97
Poisonings	72,370.53
Heat (hot and cold exposure)	53,349.52
Terrorism	26,445
Natural disasters	9,602.94

Source: IHME, Global Burden of Disease   OurWorldInData.org/causes-of-death • CC BY

Figure 1.1: Worldwide death rates due to different disorders [1].

Cancer is a term used to describe a collection of diseases that have similar origin. That is, in all types of cancer, the mechanism of division of some body cells starts functioning wrong at some point, and the cell starts to divide unstoppably and uncontrollably. Consequently, as there are more new cells than the system requires, these cells start to invade the neighbouring tissues. This phenomenon is related to the fact that cancer cells are not as highly specialized as normal cells, therefore,

they can relatively easily break into different tissues. Having stated that, it should be mentioned, that it is very difficult, if not impossible, to predict, where cancer may start, as nearly all cells in the human body use the same mechanism of division, which could start functioning wrong at some point and give rise to a tumor.

Cancer is a disease that can have many reasons, both genetic-related and individual-specific. Speaking of genetics, the mechanism of cell division is encoded in the human DNA (Deoxyribonucleic Acid), and the changes in genes may influence the way how cells divide or function. These changes may be inherited from the parents of an individual or arise during one's lifetime. Factors affecting this process are long-term exposure to ultraviolet light, tobacco smoke, continuous and long-term contact with chemicals, etc. What makes some cases of cancer even more difficult to treat is the possibility of occurrence of the gene-changing process within an already growing tumor. This means that different cells will have undergone different mutations, making each case of cancer unique and the condition itself very individual-specific [8].

The majority of cancer types are located in the abdomen – the area in the body between thorax and pelvis. It contains all the digestive organs, kidneys, the mesentery and the spleen [9]. According to statistics, here occurs one of the deadliest cancers – the pancreatic cancer, which has a survival rate of only about 7 % [10]. Other abdominal organs affected by this disease include the stomach, esophagus, lungs and liver. The survival rates for each of them are presented in Figure 1.2.

As there is a great variety of cancer types and the requirement for individual-specific approach towards each case that has been introduced earlier, the methods used to treat cancer also vary greatly. Due to cancer being a very complex disease with almost unpredictable speed of development, most often, a combination of different methods is used to treat it. For example, this could be the simultaneous use of chemo- and radiotherapy. Most used methods of cancer treatment include direct surgical intervention, chemotherapy, radiotherapy, immunotherapy, hormone therapy, targeted therapy and hyperthermia [11].

Up to these days, chemotherapy, radiation therapy and direct surgical tumor removal were the main methods used to treat and cure cancer. However, the negative side effects of these methods have always been of great concern both to physicians and patients. Namely, these include the feeling of fatigue, hair loss, constipation, anemia, easy bruising and bleeding, changes in the digestive tract [12]. For this reason, aiming to make the process of cancer treatment less unpleasant for the patient, researchers and doctors have been looking for a less toxic and harmful way to treat this disease. After the investigation of cancer cells and their properties, it has been concluded that thermotherapy or hyperthermia could be a very promising approach towards cancer treatment, especially, when used in combination with other

Cancer deaths by type, World, 2017

Total annual number of deaths from cancers across all ages and both sexes, broken down by cancer type.

Cancer type	Deaths
Tracheal, bronchus, and lung cancer	1.88 million
Colon and rectum cancer	896,040
Stomach cancer	864,989
Liver cancer	819,435
Breast cancer	611,625
Pancreatic cancer	441,083
Esophageal cancer	435,959
Prostate cancer	415,910
Leukemia	347,583
Cervical cancer	259,671
Brain and nervous system cancer	247,143
Bladder cancer	196,546
Lip and oral cavity cancer	193,696
Ovarian cancer	175,982
Gallbladder and biliary tract cancer	173,974
Kidney cancer	138,526
Larynx cancer	126,471
Other pharynx cancer	117,412
Multiple myeloma	107,114
Other cancers	102,920
Uterine cancer	85,239
Nasopharynx cancer	69,550
Non-melanoma skin cancer	65,097
Malignant skin melanoma	61,665
Thyroid cancer	41,235
Hodgkin lymphoma	32,560
Testicular cancer	7,662

Source: IHME, Global Burden of Disease (GBD)   CC BY

Figure 1.2: The deadliest cancer types located in the abdomen [1].

conventional methods like radio- or chemotherapy. This conclusion is based on the established properties of cancer cells that are affected by high temperatures. The implementation of this concept in clinical practice led to positive results, which can be seen by looking at Figure 1.3.

In order to describe the essence of the hyperthermic method in greater detail and understand the patient's benefit from the use of it, it is, at first, necessary to understand the underlying mechanism or the fundamental principle of the method. In simple words, hyperthermia means repeated heating of the tumor area by temperatures ranging from 41 to 45 °C. The problem with standard working environment (25 °C) is that it makes radio- and chemotherapy less effective because a significantly smaller concentration of the drug will reach the required area, and the radiation dose that will have reached the tumor area is going to be remarkably lower compared to the initial one. On the contrary, treatment under temperatures ranging from 41 °C to 45 °C, according to conducted research [13], is toxic for cancer cells which have low pO_2 (Partial Pressure Of Oxygen) and low pH (scale used to specify the acidity or basicity of an aqueous solution) due to poor perfusion. At these temperatures cancer cells experience significant damage to the DNA, protein denaturation and other effects [14]. Therefore, with the use of hyperthermia as an addition to conventional methods, notably better results can be achieved due to physiological
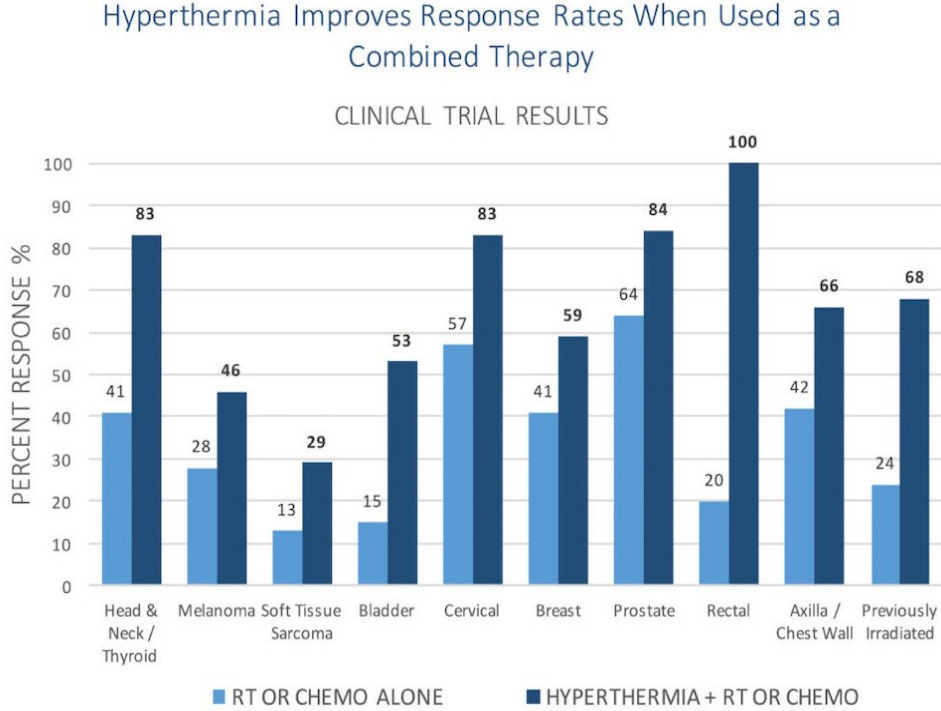
Figure 1.3: Response rates of patients with cancer to the use of hyperthermia in combination with radio- or chemotherapy [2]. *Note: the original image has been edited.*

properties of blood related to temperature increase. The delivery of heat leads to increased perfusion, therefore, it increases the drug dose that reaches the tumor. Furthermore, less radiation will be required, which is another benefit for the health of the patient [15].

The increase in temperature in the tumor area can be achieved either by the use of ultrasound waves or MW (Microwave) EM (Electromagnetic) radiation. In this thesis we will focus on hyperthermic systems which work only with MW EM radiation. Depending on the type of cancer and the concrete patient case, hyperthermia can be applied in three different ways – local, regional and whole-body hyperthermia. The applicator for hyperthermia is the spatial geometric arrangement of one or more antennas. The configuration of the array of applicators or antennas allows for the control and variation of the generated MW radiation. For proper treatment, it is necessary to adjust the MW distribution for the concrete case of a particular patient. This is done by setting the applicator parameters – the number and placement of antennas in the array, frequency, amplitude and phase of the MW emitted by each antenna in the array, etc. Although the choice of number of antennas in the array may be a relatively easy task, their placement and frequency, either empirically or by experience, the determination of amplitudes and phases of individual applicator antennas is a problem that is better to address with the help of special optimization

algorithms. The aim of the whole array setup is to distribute the maximum possible amount of energy to the tumor area while not exceeding the threshold temperature to the other tissues to avoid the feeling of pain and discomfort for the patient [16].

The key parameter for the focusing of MW is the choice of phase of each antenna, which influences the MW interference in the whole system. After setting the phase, the amplitude of each antenna determines the total energy that is transferred to the tumor location and to the surrounding tissues. From this follows that the main goal of optimization tasks in hyperthermic cancer treatment is the search of phases and amplitudes of individual antenna elements to distribute the desired amount of energy to the location of interest. Optimization tasks in hyperthermia treatment seek to determine such amplitudes and phases of individual antennas so as to meet the physician's requirements. At this point, it is important to choose the criteria function, i.e., the criterion that determines how the computations of the optimization algorithm are judged. The entire process from the acquisition of the tissue image to the determination of the system parameters is referred to as HTP (Hyperthermia Treatment planning), which is further to be discussed in greater detail in the following chapter.

Although MW EM technique in hyperthermia is also a form of radiation and does exhibit some toxicity, it is significantly smaller than that of chemo- and radio-therapies. The recent advances in heating techniques and thermometry, development of hyperthermia treatment planning models, research studies on heat shock proteins - all promise a bright future to hyperthermic cancer treatment.

2 Overview of the current state

This sub-chapter is aimed to describe the state of the art of hyperthermic cancer treatment. Main hyperthermic methods and techniques will be introduced and discussed in detail along with their strong sides and imperfections. Likewise, the essence and the application of HTP in modern clinical practice will be mentioned.

2.1 Hyperthermia in modern clinical practice

Hyperthermia in a medical sense means the application of either microwaves or ultrasound for tens of minutes until the temperature of the tumor reaches the value of approximately 40-44 °C. Although ultrasound has similar tissue heating properties like MW, the physical nature of reflection of mechanical waves results in a greater feeling of pain and discomfort in patients, when the waves strike the interface between bone and surrounding tissues [17]. Moreover, it is very unlikely that the HT (Hyperthermia) system will be able to heat the entire volume of the tumor to 43 °C and above while still maintaining a tolerable temperature in the surrounding tissues [18]. For this reason, HT is not used alone but always in combination with radio- or chemotherapy.

2.2 Biological effect of hyperthermia

Heating the tumor to a temperature of 40-42 °C does not kill cancer cells but does have a significant harmful effect on them. Like high fever, HT increases the immunological activity of the human body. Besides, there is an increase in tumor perfusion, meaning more blood and more oxygen is supplied to the tumor. Insufficient perfusion results in poorer efficacy of cytostatics in HT, and hypoxia of tumor cells is considered to be the reason of their resistance to RT (Radiotherapy) [19]. Consequently, HT increases tumor sensitivity to RT or chemotherapy. During RT, radiation photons or other particles strike the DNA structure of the target cell, while chemotherapy destroys dividing cells with chemicals. Temperatures above 41 °C inhibit the mechanisms responsible for repair of damaged DNA, therefore, increasing the effectiveness of the dose. In other words, malignant cell's proteins denaturate when presented to temperatures within the hyperthermic range and subsequently destabilize the intracellular environment together with DNA repair system [20]. The harmful effect of hyperthermic temperatures on cancer cells can also be magnified by environmental and vascular conditions. In normal, healthy tissue the dilating vessels increase the blood flow in specific region and thus decrease the temperature, as blood carries away the excessive heat. In tumor, on the contrary, the pathological vessels cannot dilate, which results in higher sensitivity to heat [20].

2.3 Hyperthermic techniques used in tissue heating

Depending on the position, depth and staging of the tumor, there appear to be three different types of hyperthermia treatment: local, regional and whole-body hyperthermia.

In local HT the heat is distributed to a very small area, ideally, only to the tumor. It can be further subdivided into external, intraluminal (endocavitary) and interstitial, depending on the tumor location. In the external approach, as the name suggests, tumors located in or on the surface of the skin are treated by placing the external energy applicators around the tumor area to focus on it and heat it up. Intraluminal method is used to treat tumors located near or inside body cavities like rectum and esophagus – the main tool are the probes which are inserted into the tumor in the appropriate body cavity to heat this area directly. Interstitial method is used to treat hardly accessible tumors located deep in the body, such as brain tumors. It relies on probes and needles inserted into the tumor under anesthesia. Another example of an invasive technique is the use of magnetic particles applied directly between tumor cells. A time-varying magnetic field induces electric current between the particles, which, in turn, heats the tumor [21].

A future potential powerful tool that can be used in local or regional HT is HIFU (High-intensity Focused Ultrasound) beam. It is controlled by either MR (Magnetic Resonance) or CT (Computed Tomography) and delivers large amounts of energy to the tissues, increasing their temperature up to 65-85 °C. By means of such high temperature it destroys unwanted tissue by ablating it with millimeter precision. Nowadays, this technique is mostly used in neurosurgery and to treat malignant and benign tumors [22].

Regional HT is used to treat tumors localized at a depth of at least four centimeters [23]. For example, deep seated tumors within the pelvic region like cervical, rectal, bladder or prostate cancer, belong to the types for the treatment of which the regional approach is advisable [20]. It was shown in [24] that the three above-mentioned cancers have an increase in the therapeutic response (the disappearance of all cancer signs and symptoms as a result of treatment) from 39 to 55 % when adding hyperthermia to radiotherapy. In 2017, more than 1.7 million people died worldwide due to cancer in the pelvic region, numbers in the Czech Republic reach the value of 7 thousands [1]. If a closer look is taken at the survival rates for these types of cancer over the five-year period, one can see that they exhibit higher values of this parameter (cervix – 64.5 %, prostate – 83.1 %, rectum – 51.3 % [1]) than many other cancer types in the Czech Republic in particular, however, the situation can still be improved.

As the name suggests, regional type of hyperthermia involves heating healthy tissue along with the tumor. Therefore, the main task in regional HT is to heat the tumor volume more than the surrounding tissue. To resolve this, an array of individual antennas and an interference effect can be used, where the proper adjustment of individual antennas allows for having a composite field with maximum amplitude at almost any location.

Targeting tumors that are seated deeper inside the body may require the use of lower frequencies (approx. 70-150 MHz). Such frequencies allow for greater depth of penetration, but a larger wavelength, on the other side, leads to a decrease in the resolution of the interference range, which means it will be harder to target details [25].

A bolus filled with flowing water is usually placed between the patient and the applicator. There are two main reasons for that: 1) reducing temperature on the surface of the body and thus preventing skin burns and 2) ensuring good impedance matching. The choice of water temperature depends on the depth of the tumor location (commonly used temperature is about 10 °C [26]). If possible, it is advisable to use distilled (deionized) water, the conductivity of which is lower by the order of magnitude, creating a better medium for energy transfer. In [27] it has been shown that the thickness of the water cushion has a negligible effect on the overall energy distribution, as long as the layer is thick enough to provide uniform cooling.

Finally, whole-body hyperthermia is used to treat metastatic cancer which has spread throughout the body. It is typically used together with chemotherapy. It means, this approach is not suitable for the primary stages of cancer. The increase of temperature can be achieved by conventional heating of the skin with infra-red radiation, thermal chambers, hot air, water or wax. There is also a possibility to perform extracorporeal heating of the blood, but there is evidence that it may result in undesirable changes in the coagulation system [28].

2.4 Imperfections of today's hyperthermic cancer treatment

The medicine of today made it possible to diagnose cancer at an early stage and start the treatment without delay. Therefore, many hyperthermic systems nowadays are locoregional. They consist of a large number of RF (Radiofrequency) antennas, organized in multiple rings. These antennas surround the patient and, consequently, heating of the normal healthy tissue along with the tumor occurs. An example of the equipment used in modern hyperthermic cancer treatment is presented in Figure 2.1.

Although hyperthermia in general is an effective treatment method, which follows from numerous research works and experiments, there are some drawbacks.

Figure 2.1: Example of equipment used in microwave hyperthermic treatment [3].

Mainly, they are connected with treatment limiting hotspots in normal tissue. These hotspots impede the increase in total power delivered to the patient, meaning the applied temperature does not imply 100% efficiency because some of the power is dissipated in healthy tissues before it reaches the tumor. Today, the prevention of the influence of such hotspots is of great importance in the construction of hyperthermic systems as it directly influences the clinical outcome.

There are two main aspects which govern the process of hyperthermic cancer treatment – active treatment control and spatial power control. The former accounts for the influence of the hotspots and aims to reduce their influence. It is highly temperature dependent and relies on the information received from minimally invasive thermometry probes. NIT (Non-Invasive Thermometry) approach is a helpful tool to get a deeper insight into the quality of heating, however, it is not generally available and results in inaccuracies in case of moving tumors. Moreover, difficulties with its exploitation may arise when metal structures are used in the construction of the heating equipment. Nowadays, there is a great interest in using NIT combined with CT, as CT technologies quickly advance [29]. Spatial power control depends on the number of antennas used and the operating frequency. The higher the number of antennas and frequency, the better steering can be achieved. However, despite the fact that high frequencies let focus on the small volume and give good precision, the penetration depth is small, which implies that more antennas are required, otherwise deep-seated tumors cannot be reached and treated properly. Additionally, it is difficult for the operator to deal with a large number of antennas and adjust phase and amplitude of each of them. To resolve these issues, HTP has been introduced

as an instrument that deals simultaneously with power absorption and temperature patterns by simulation and aims to give the operator an adequate visualization of different steering strategies. Besides, numerical optimization techniques are used to correctly set the amplitudes and phases by accounting for user-defined limitations connected with temperatures and power absorption in normal, healthy tissues. Step by step, HTP simulation has gone from a research tool to an irreplaceable part of clinical cancer treatment [30]. The following sub-chapter summarizes and discusses in greater detail the algorithm of HTP.

2.5   Algorithm of HTP

Typically, in the process of microwave or RF hyperthermia treatment planning the following steps can be distinguished:

1. Tissue segmentation for dielectric and thermal model generation

2. Electromagnetic field simulation

3. Temperature calculation

4. Phase-amplitude optimisation

Each step has a variety of different methods available for its simulation, depending on accuracy, modelling complexity and clinical usefulness.

Tissue segmentation is a very important part of HTP. It considers the dielectric properties of different tissues which limit the energy absorbed by the tumor by dissipating it. Therefore, it influences a lot the simulation results. Segmentation is performed with the help of MRI (Magnetic Resonance Imaging) or CT manually or semi-manually in the same position of the patient as for hyperthermia treatment. The advantage of MRI over CT is that it has much better contrast in case of soft tissues. Figure 2.2 provides an example of difference in quality of imaging brain tissues by both techniques for comparison.

One of the techniques is automatic segmentation based on Hounsfield units. It helps to distinguish between tissue types with large dielectric constants like water, fat, bone tissue, etc., however, it is able to lead to inaccuracies when it comes to organs with similar densities but different dielectric properties, e.g., liver and kidneys.

A more accurate approach is connected with absorbed power calculations based on manually delineated dielectric models. It is a complex method because delineation of normal tissue has high requirements due to a large variation of dielectric
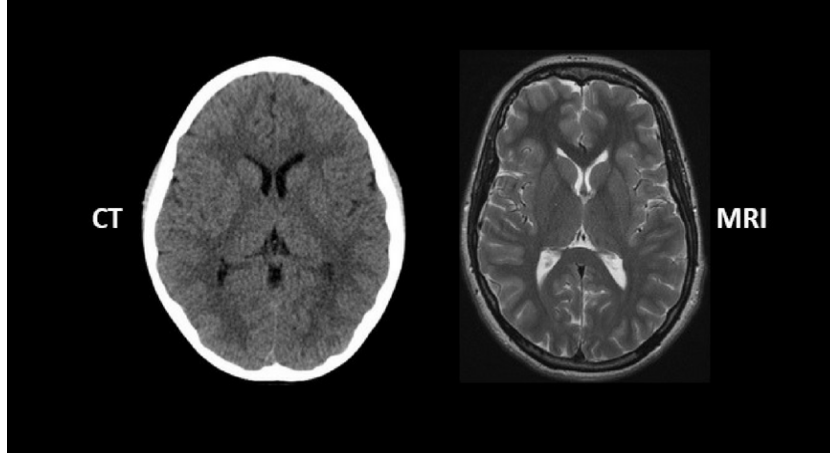
Figure 2.2: The quality difference between CT and MRI scans of the brain [4].

and thermal properties in different organs, as well as electromagnetic boundary conditions. Manual delineation is also associated with long operator time.

A relatively new segmentation technique applied in the areas of head and neck involves the combined use of CT and MRI. It has been proved that MRI helps provide more accurate delineation of the brain, while having no significant effect on the simulated absorbed power, and provides accurate temperature predictions. This method has earned the name of CT-MRI atlas-based delineation for head and neck hyperthermia and is currently under development. Such atlas-based approach has not yet been introduced for the pelvic region. Patient-specific HTP can be done via tissue segmentation of one particular person. In this approach, dielectric imaging techniques that reconstruct a full 3D (Three-Dimensional) distribution of the patient's dielectric tissue properties are investigated. The method proposed for this is a two-step dielectric imaging: first the water and fat contents are determined using standard MRI techniques, then the water contents are converted to permittivity maps. This method is still under investigation, as it provides quite significant variations in case of several tissues [30].

The creation of the dielectric model of the patient is then followed by the calculation of the EM field distribution in that patient. This is done by numerically solving Maxwell's equations. To elevate the accuracy, the positioning of the patient is crucial. For an operating frequency of 70 MHz the deviation of the patient's position in the heating system of HTP from his position during clinical treatment should not be greater than 1-2 centimeters. Higher frequencies require even greater precision due to smaller wavelengths and hot spots. In order for the treatment to be effective, the reflection of the EM waves at the boundaries of the computational domain should be prevented. Therefore, absorbing boundary conditions are necessary. Today, PML (Perfectly Matched Layer) is the most effective variation of ABCs (Absorbing Boundary Condition(s)). Its outlook can be seen in Figure 2.3.
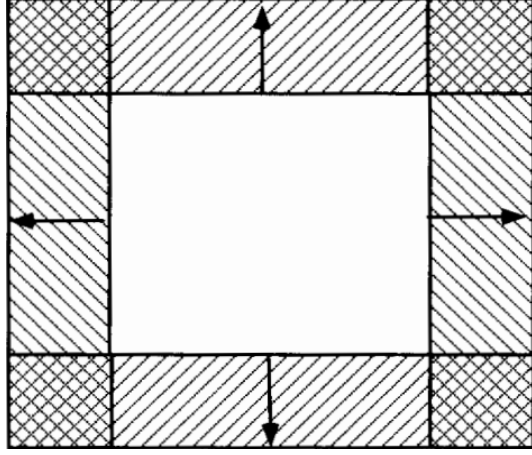
Figure 2.3: The outlook Of PML (dashed areas) [5].

In modern practice, either differential or integral methods of solving Maxwell's equations are available for the simulation of EM fields distribution. FDTD (Finite-Difference-Time-Domain) and FE (Finite Element)methods are considered the most popular. FDTD uses discretization of the computational domain into rectangular voxels. For accuracy reasons, at least 10-20 voxels per wavelength should be used. FDTD is based on the Yee cell, in which the electric field components are on the edges of the voxel and magnetic field components are on the faces, or the other way around. The electromagnetic field propagation is calculated for successive time steps, until steady state is reached [31]. The basis of this method is the consideration of the displacement of the E-field (electric field) with respect to the H-field (magnetic field) by half a unit in both time and space. The unknown value of the E-field (or H-field) is calculated as a central difference using the value of the previous time step and the value of the neighboring points [32].

Considering Maxwell's equations for the E-field and H-field in a simplified air medium:

$$\frac{\partial E}{\partial t} = \frac{1}{\varepsilon_0} \nabla \times H \tag{2.1}$$

$$\frac{\partial H}{\partial t} = -\frac{1}{\mu_0} \nabla \times E \tag{2.2}$$

where E $[\text{V} \cdot \text{m}^{-1}]$ is the electric field intensity, H $[\text{A} \cdot \text{m}^{-1}]$ is the magnetic field intensity, t [s] is the time unit, ε_0 $[\text{F} \cdot \text{m}^{-1}]$ is the permittivity of the environment in which the EM wave is propagating and μ_0 $[\text{H} \cdot \text{m}^{-1}]$ is the permeability of this environment. Equations (2.1) and (2.2) would have to be complicated by the introduction of material coefficients in case of more sophisticated propagation media, e.g. biological tissues.

For a simplified one-dimensional case of EM wave propagation in the direction of z-axis, it is possible to write:

$$\frac{\partial E_x}{\partial t} = -\frac{1}{\varepsilon_0}\frac{\partial H_y}{\partial z} \tag{2.3}$$

$$\frac{\partial H_t}{\partial t} = -\frac{1}{\mu_0}\frac{\partial E_x}{\partial z} \tag{2.4}$$

The idea of FDTD is to shift E_x and H_y by half the sample in both time (n) and space (k). The central difference for the free (lossless) environment can then be expressed as

$$\frac{E_x^{n+\frac{1}{2}}(k) - E_x^{n-\frac{1}{2}}(k)}{\triangle t} = -\frac{1}{\varepsilon_0}\frac{H_y^n(k+\frac{1}{2}) - H_y^n(k-\frac{1}{2})}{\triangle z} \tag{2.5}$$

$$\frac{H_y^{n+1}(k+\frac{1}{2}) - H_y^n(k+\frac{1}{2}}{\triangle t} = -\frac{1}{\mu_0}\frac{E_x^{n+\frac{1}{2}}(k+1) - E_x^{n+\frac{1}{2}}(k)}{\triangle z} \tag{2.6}$$

For example, left side of equation (2.5) shows that the central difference of the E-field at time n can be expressed as the difference of the E-field values at time instants $n - \frac{1}{2}$ and $n + \frac{1}{2}$. Right side of equation (2.5) expresses the central difference of the H-field at point k as a difference of the H-field values at points $k - \frac{1}{2}$ and $k + \frac{1}{2}$. Using these equations, it is, therefore, possible to calculate the value of the E field (or H-field) at time $n + \frac{1}{2}$ given the values at time $n - \frac{1}{2}$ and the values of the neighbouring points at time n.

The main and, perhaps, only significant drawback is the appearance of "staircasing" when it comes to simulating EM field propagation at very irregular and geometrically detailed tissue interfaces. There are methods how to deal with this issue, however, it would be at the cost of increased complexity and computation time.

The FE method provides better accuracy than FDTD but is much harder to implement – it requires a special software which would divide the computational domain into tetrahedral or hexahedral elements – see Figure 2.4. Higher accuracy is due to the use of trial functions which are applied to partial differential equations to minimize the error. The field equations are represented by polynomials with unknown coefficients, which are determined by solving a sparse matrix equation [30].

Regarding the integral techniques, one can name FIT (Finite Integration Technique), VSIE (Volume Surface Integral Equation) and WF-CGFFT (Weak Form
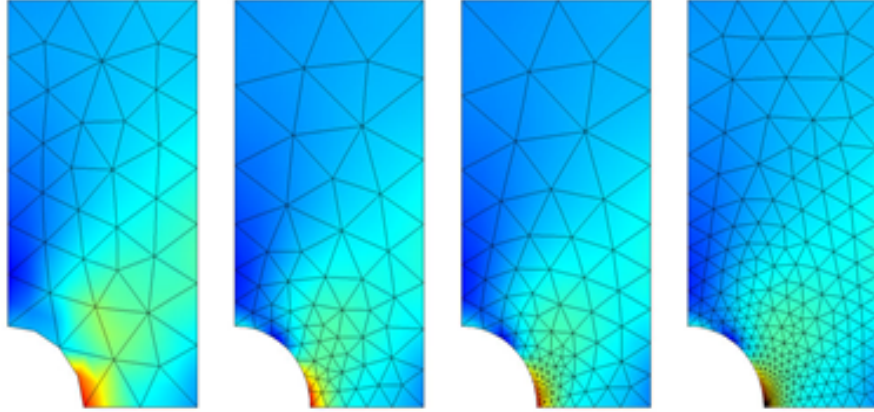
Figure 2.4: An example of FE triangular mesh used in simulations involving the
Finite Element method [6].

of the Conjugate Gradient Fast Fourier Transform). FIT is the generalization of
FDTD and also resembles FE, it can be used both with rectangular and tetrahedral
meshes. The integral equations are converted into a block of matrix equations on
an orthogonal dual grid pair. The electric grid voltage and magnetic facet flux are
defined on the primary grid and magnetic grid voltages and electric facet fluxes are
defined on the second grid. The transient solver is predicated on the result of solving
these matrix equations, which yields a fully unequivocal time-stepping procedure as
in the FDTD method. The FIT is truly flexible in geometric modelling and handling
of boundaries. VSIE has been proposed to be applied on region-based segmented
patient model, discretized on a tetrahedral mesh. This is one of the drawbacks –
a software is needed to generate such mesh. Its biggest advantage is the accuracy,
provided that tissue interfaces have been described properly by the grid. In such
case, the integral equation is divided into a volume integral and surface integral.
Due to the computational complexity, VSIE is less efficient than FIT. WF-CGFFT
is realized on the domain with rectangular volume elements. In this method the
domain-integral equation is weakened by testing and expansion. The resulting weak
form of the integral equation is next used as input for the CGFFT method.

Following EM field simulation, comes thermal modelling - a very important aspect of HTP, as it describes the 3-D temperature distribution within the patient. It is
determined by SAR (Specific Absorption Rate) deposition and cooling mechanisms
which include perfusion, thermal and bolus cooling. Perfusion is the most significant cooling mechanism, as blood flow causes significant heat removal. Thermal
simulations nowadays are based on tabulated values of perfusion, which, however,
have some uncertainty. Despite this, it is still a challenge to conduct 3-D perfusion measurements, therefore, these uncertainties should be taken into account. At
present, there exist two main types of thermal models – continuum models and discrete vasculature models. The former are the models in which perfusion is described

26

by a continuum flow model. The most popular method used within this technique is the bioheat transfer equation, proposed by Pennes [33]. This model describes the impact of perfusion by an isotropic heat sink, commensurate to a non-directional volumetric average perfusion rate and local temperature rise. It does not account for heat exchange between tissue and realistic vasculature and does not consider the direction of the blood flow.

In discrete vasculature models thermally significant blood vessels are modeled discretely to predict local temperature inhomogeneities. These models show that heat transfer between large thermally significant blood vessels and tissue is significant and should be accounted for in hyperthermia treatment planning. The most widely-used model today is DIVA (Discrete Vasculature).

In the final part of HTP comes the phase-amplitude optimisation, the main aim of which is to find the optimal phase and amplitude for each antenna in the system such that the tumor of interest would be heated, while the influence of the hot spots in healthy tissue would be minimised. Today's optimisation strategies are divided into SAR-based and temperature-based methods. SAR is temperature-dependent, therefore, it can be used to reach the desired temperature of the tumor. However, its main drawback is the difficulty to account for the cooling mechanisms. Modelling of perfusion, conduction and bolus heating is essential to setup the antennas to avoid treatment limiting hot spots. Temperature-based optimisation maximizes the tumor temperature with the use of either soft or hard constraints to normal tissue temperatures. During the optimisation process a substantial number of temperature calculations are performed. Calculation by solving the corresponding differential equation is extremely computationally intensive and, therefore, efficient methods have been developed. Temperature-based optimisation methods are usually based on Pennes's bioheat model, as this is computationally least expensive [30].

2.6   Software in HTP

Since the use of HTP is growing rapidly, the number of corresponding software is increasing as well. The most widely used commercially available software for lo-coregional HTP planning is Sigma HyperPlan. It works on FE method but FDTD modules are also available. Other, more flexible planning systems include AMC DIVA (AMC, Amsterdam, The Netherlands) and SEMCAD X (SPAEG, Zurich, Switzerland). These allow thermal modelling, SAR calculation, phase-amplitude optimisation based on either SAR or temperature. Basic electromagnetic calculations and thermal simulations can be done by using general purpose commercial software packages such as COMSOL, Ansys High Frequency Structural Simulator, CST STUDIO SUITE. For more advanced calculations, additional software is re-

quired. Because commercial software is mainly of general purpose, even though it is developing quite rapidly, for some of the clinical applications like adaptive HTP additional software tools will be needed [30].

3   Aims of thesis

For highlighting the positive influence of microwave hyperthermia on cancer treatment processes, the aim of this thesis is to create a two-dimensional anatomically and didelctrically realistic patient model in MATLAB [34] environment and use the numerical simulator of the electromagnetic field to calculate electric fields from each antenna element of the hyperthermia system targeted at the pelvic region. The simulator is based on the FDTD method, which was chosen due to its simple implementation, calculation efficiency, and suitability for realistic patient models. It is a numerical method which, thanks to its clarity and simplicity, has become a widespread tool used in investigation of and teaching the electromagnetic field and its properties at universities and other academic institutions around the world. Thus, a big number of resources is available on the topic which can help in making the simulator meet the requirements of the realistic patient model as much as possible.

Pelvic region was chosen because tumors located in the pelvis are in general hardly accessible, and hyperthermic treatment, therefore, could be an effective and non-invasive therapy. Another reason for choosing the pelvic area was the aim of this thesis to contribute to the development of a regional hyperthermic system for the treatment of tumors in the pelvic area. Because hyperthermia systems require proper steering of all antenna elements, the development and integration of electromagnetic field simulator in this process is a very important part of the hyperthermia treatment planning. Moreover, the use of the treatment planning algorithm to optimize the complex amplitudes of the antenna signals and focus the field on the tumor within the model will make another contribution to the increased accuracy of the developed numerical simulator. The developed FDTD-based numerical simulator and the dielectrically and anatomically realistic model of the pelvic area will be used to evaluate the performance and treatment planning quality of four optimisation algorithms - THQ driven global optimisation, generalized eigenvalue approach, time-reversal and target centre point steering for 10 different target locations. Evaluation will be based on corresponding SAR distributions, clinically used parameters TC25 and TC50, and value of the THQ.

At first, a two-dimensional numerical realistic model of the pelvic area will be created in MATLAB environment. It will include all the tissues and organs present in a real human. Besides, the water bolus will be added to the computational domain as a part of the hyperthermia system. The medium surrounding the patient model will be made up of air entirely, including its dielectric properties. The next step will be the beginning of domain adjustment for the simulator of electromagnetic field - the addition of ABCs. They are necessary to obtain the clear view on how the

electromagnetic field is distributed, i.e., get a visualization without reflections at the boundaries of the computational domain. This will be done by using the PML technique. It is considered to be the best variation of ABCs nowadays as it provides great precision and allows the user to make the length of the perfectly matched layer custom without affecting the output quality. The entire computational domain will be surrounded by perfectly matched layers in x and y directions to prevent unnecessary reflections at the boundaries.

The last step in making the patient model realistic is assigning each organ and tissue proper values of the corresponding dielectric properties (relative permittivity, electrical conductivity) and density. These parameters are necessary for the evaluation of essential physical quantities involved in electromagnetic field calculation and also the SAR. Finalizing the setup of the computational domain, four antennas will be added on the surface of the water bolus surrounding the patient model. The source operating frequency was chosen to be 70 MHz because lower frequencies allow for greater depth of penetration, which is the case in pelvic cancer treatment.

Summing up all of the mentioned above, it is possible to conclude that the main aim of this project is the development of a two-dimensional numerical simulator in MATLAB environment which would calculate as accurately as possible the distribution of the electromagnetic field at any given spatial point in the computational domain (any point in space in the hyperthermic system) containing anatomically and dielectrically realistic model of pelvic area of a patient for given values of amplitudes and phases of signals applied to individual antennas. In order to prove this, the same model will be created in a commercial simulator COMSOL Multiphysics to compare the results of the two and verify the validity of the developed numerical simulator which was created with the help of the FDTD approach [35]. The validated simulator is to be used for studying four treatment planning algorithms by means of clinically used parameters TC25 and TC50.

4 Methods

4.1 Development of 2D FDTD-based simulator for a simplified model of pelvic area

Fulfilling the aims of this project requires iterative work in MATLAB environment. The first step in the creation of a two-dimensional simulator was the implementation of the transverse magnetic mode [36] which includes E_z, H_y, and H_x fields in the medium made up of air only. This approach was necessary to test whether the algorithm would function correctly in a simple medium before introducing more complex patient models to the simulation. The ultimate goal of using the mentioned transverse magnetic mode is to model the behaviour of the E_z field. Because the FDTD method is iterative and uses calculation of E-fields from H-fields and vice versa, there was a need to normalize both these fields by a factor of $\sqrt{\epsilon_0 \cdot \mu_0^{-1}}$, where $\epsilon_0 = 8.85 \cdot 10^{-12}$ is the vacuum permittivity in $[\mathrm{F} \cdot \mathrm{m}^{-1}]$ and $\mu_0 = 4 \cdot \pi \cdot 10^{-7}$ is the vacuum permeability in $[\mathrm{H} \cdot \mathrm{m}^{-1}]$ so they would have similar amplitudes. The reason for that was the initial big difference in magnitudes of these fields in the range of several orders – this could potentially lead to numerical errors during the execution of the algorithm.

Regarding the ABCs, for two-dimensional problems the most suitable approach is the PML, whose structure was adopted from the relevant literature source [37] and modified to suit the concrete case of this thesis. Although the way of implementation is different from the approach used for one-dimensional simulations, the main aim remains the same – to remove reflections from all four outer boundaries of the domain (left, right, top, and bottom boundaries). After setting the ABCs, the four antennas were placed in the domain in such way that later they could surround a patient model. All of them had the same operating frequency of 70 MHz. At this point, the accuracy of the simulator was tested by plotting the electromagnetic field distribution with all sources turned on to verify that its performance meets the real requirements.

The correspondence of results with the expected behaviour of the electromagnetic field distribution led to the introduction of the patient model to the simulation. It was chosen to be an elliptical model, as the ellipse better corresponds to the real patient than the alternative dielectric cylinder option. This was achieved by implementing the ellipse equation to the code and defining the relevant relative permittivity and electrical conductivity values for each spatial step the ellipse was meant to occupy. The creation of a matrix with all the material properties was used to define the necessary relative permittivity and electrical conductivity values at each spatial step in both x and y directions. The dimensions of the semi-axes of the ellipse (and therefore the thickness of the model) were the same as the ones created with the help of a commercial simulator COMSOL Multiphysics (the procedure is discussed later in this section) as a means of verification of the validity of the developed numerical simulator. The model was set to two layers – one for water bolus (cooling unit) and another for human muscle tissue. Skin and fat layers were omitted at this point of simulator development due to insignificant effect on the overall simulation result due to small thickness and from the point of view of speeding up the computation in MATLAB, because numerous looping algorithms incorporated in such complex problem even for thin layers are time-consuming. The surrounding medium outside the model was initially set to the parameters of air, making it a total of three materials present in the simulation – air, water, and human muscle tissue. Moreover, the overall domain area was set to 1.4 x 1.4 meters which corresponds to the realistic dimensions of hyperthermia systems used in modern clinical practice. Furthermore, various parameters were changed in the setup of the antennas. At first, three out of four antennas were deactivated and only the top applicator was left active. Since optimization of sources is not yet the main task at this point, simulating the activity of one source eases the investigation of the E-field propagation in terms of its phasor. Evaluating single source activity in terms of SAR is also appropriate, since in reality during the setup of the hyperthermic system each antenna is calibrated separately, with its value of SAR being of the greatest interest. Secondly, source type was changed from soft, which was used up to this point, to hard in order to remove undesired big step-like changes from positive to negative values in the SAR monitored on the surface of the water bolus. This was done by setting the E-field at the position of the source. The maximum SAR value was identified from the simulation and used as a normalization factor for the overall SAR distribution throughout the model so that the maximum SAR value would be equal to one. These additional modifications were the final step in the development of the simulator in MATLAB.

The last step of the process of developing a simplified simulator was the creation of the same model in a commercial simulator – COMSOL Multiphysics. This simulator was chosen due to its accuracy, availability for our faculty, flexibility, and

speedy performance. The model was created using all parameters of the FDTD prototype. The model was made up of one rectangle responsible for the entire domain filled with air including its dielectric properties and of two ellipses, one for the water bolus and one for the patient (muscle tissue) - see figure 4.1. The four sources were positioned at the interface of the water bolus and air, they were chosen to be cylindrical sources. Then, three of them, except for the top antenna (source 2), were deactivated, as it had previously been done in MATLAB. Since the E-field phasor and the SAR distribution would be normalised with respect to the maximum value, input power of the active source was set to $1 \text{ W} \cdot \text{m}^{-1}$, as this could not affect the simulation result. As in MATLAB, phase setting of the active source was set to 0.45 radians. Scattering boundary condition with no incident field and scattered plane wave type of the first order was implemented. After this was done, the results of the two simulations were compared and analysed in terms of normalised magnitude of the E-field phasor and SAR distributions.
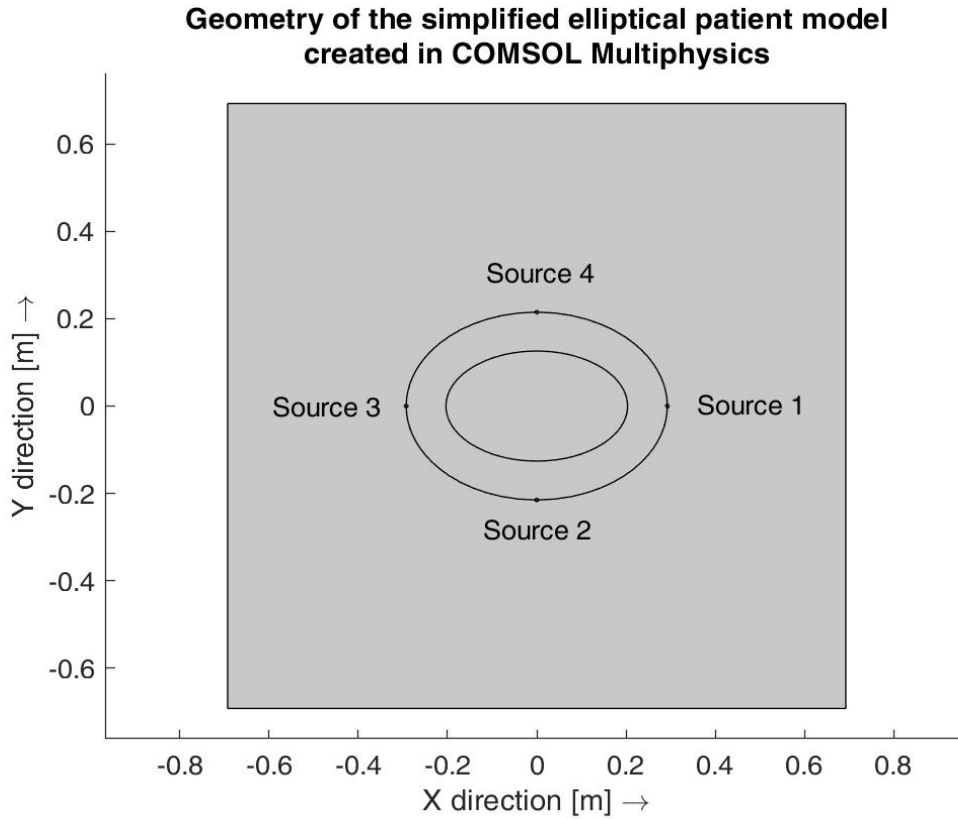

Figure 4.1: COMSOL model geometry for the case of the simplified elliptical model of the pelvic area.

4.2 Development of 2D FDTD-based simulator for anatomically and dielectrically realistic model of pelvic area

After evaluating the performance accuracy of the developed FDTD-based simulator using the commercial simulation software COMSOL Multiphysics for four parameters - electric field distribution and SAR distribution, the existing simplified elliptical patient model of the pelvic area was upgraded to a two-dimensional anatomically and dielectrically realistic version. This involved the creation of a corresponding realistic model of a human torso. It was accomplished via the use of the Zubal numerical phantom [38]. This three-dimensional phantom of the whole human body is comprised of voxels which have the size of 4 mm and represent different body tissues. For the purposes of this thesis and its focus on the pelvic region, a cross-section that includes the urinary bladder was chosen, making it the target organ for the applied hyperthermia treatment (see Figure 4.2, where the bladder and its interior is highlighted in yellow and dark-yellow color, respectively). The bladder
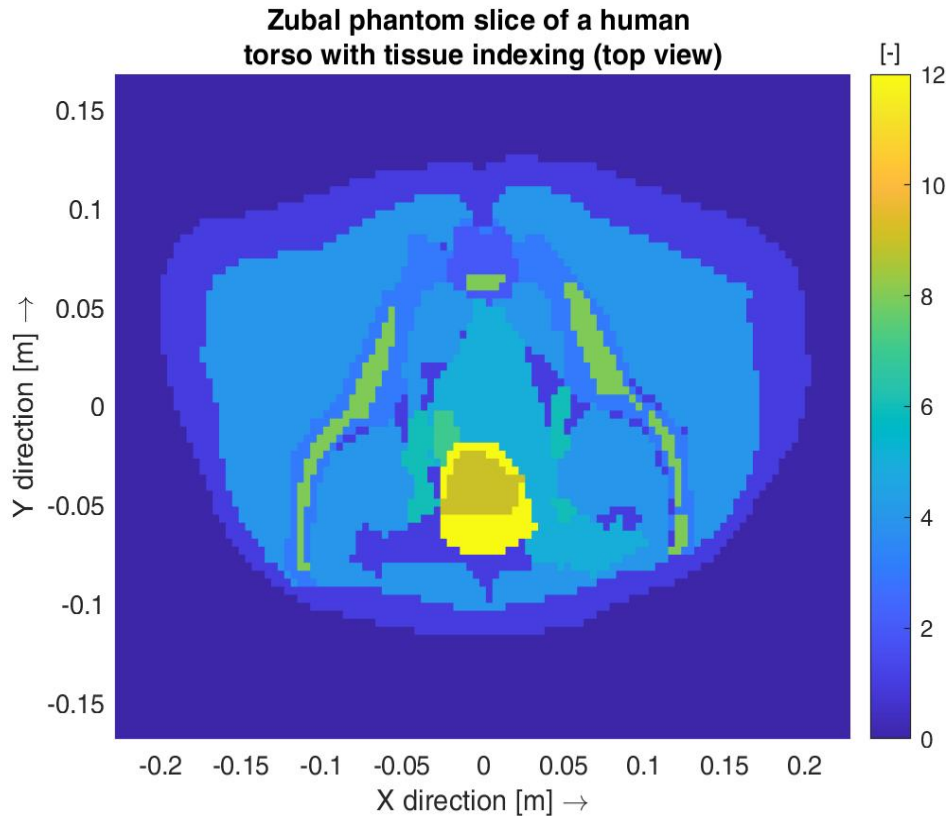
Figure 4.2: The chosen slice of the Zubal numerical phantom containing the urinary bladder for the simulation of electric field distribution.

was chosen because it is located relatively deep in the body and allows to test the created numerical simulator in a more complex and sophisticated treatment planning scenario. This means testing the case with simulating various and numerous wave propagating media (different human tissues such as skin, adipose tissue, muscle

tissue, bony structures, etc.) and also steering the system using four different beam steering strategies:

1. THQ driven global optimization,

2. Generalized Eigenvalue Approach,

3. Time-Reversal, and

4. Target Centre Point (TCP) steering

by means of optimization algorithms with regards to a more sophisticated SAR distribution in different tissues. It is important to note that the original phantom shown in Figure 4.2 contains no skin layer around the body. Therefore, it was added to the computational domain manually to make the model fully resemble the real patient. Moreover, in hyperthermic cancer treatment water bolus is an essential part of the system as it accounts for the cooling of the patient's surface to prevent burns on the skin surface and improve impedance matching. The added water bolus has an elliptical shape, and the length of its semi-axes was chosen so as to fit both the overall domain dimensions (which are appropriate for the modelling of the hyperthermic cancer treatment system and, therefore, did not have to be changed from the default settings chosen for the case of modelling the simplified model of the pelvic region) and also the patient.

The creation of a realistic patient model was followed by the implementation of the Cole-Cole model of dielectric properties of each tissue. The reason behind implementing the four-pole temperature-independent Cole-Cole model instead of inserting static parameters for one particular frequency was to make the simulator more flexible for the cases of hyperthermia treatment at different frequencies (e.g. 70 MHz, 434 MHz, etc.). Temperature dependence is not essential to implement in the particular case of this thesis, because during hyperthermia treatment the temperature increase is by 8 °C at most and can be neglected. The Cole-Cole equation enables to calculate relative frequency-dependent complex permittivity of the tissue ϵ_r, and afterwards its relative permittivity and electrical conductivity at any frequency from the considered frequency range. The extended single-pole temperature-independent Cole-Cole model [39] is described by the following equation:

$$\epsilon_r(\omega) = \epsilon_{r\infty} + \frac{\Delta\epsilon_{r,1\infty}}{1+i\omega\tau_1^{1-\alpha_1}} + \frac{\Delta\epsilon_{r,2\infty}}{1+i\omega\tau_2^{1-\alpha_2}} + \frac{\Delta\epsilon_{r,3\infty}}{1+i\omega\tau_3^{1-\alpha_3}} + \frac{\Delta\epsilon_{r,4\infty}}{1+i\omega\tau_4^{1-\alpha_4}} - \frac{\sigma}{i\omega\epsilon_0}, \quad (4.1)$$

where $\epsilon_{r\infty}$ is relative permittivity at high frequencies, $\Delta\epsilon_{ri\infty}$ is the magnitude of the dispersion, τ is the relaxation time, α is the parameter related to the broadening of the dispersion, σ is the static ionic conductivity and ϵ_0 is the vacuum permittiv-

ity. The relevant dielectric parameters for each tissue can be found in the on-line database [40].

The next step after the implementation of the four-pole Cole-Cole model and calculation of relative permittivity and electrical conductivity of all tissues that comprised the chosen slice from the Zubal phantom, these parameters were stored in separate arrays and visualized (see Figures 4.3 and 4.4). It is important to mention that in these figures the urinary bladder was chosen to be full with urine, as it is an important physiological substance that is constantly being produced by the body.
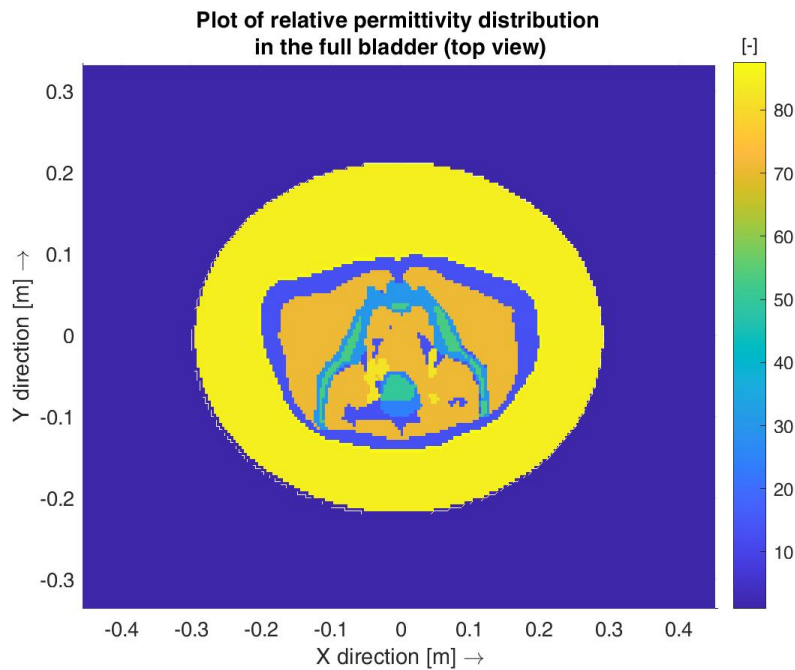

Figure 4.3: Plot of relative permittivity of the tissues within the chosen cross-section of the Zubal numerical phantom for the case of the full urinary bladder.
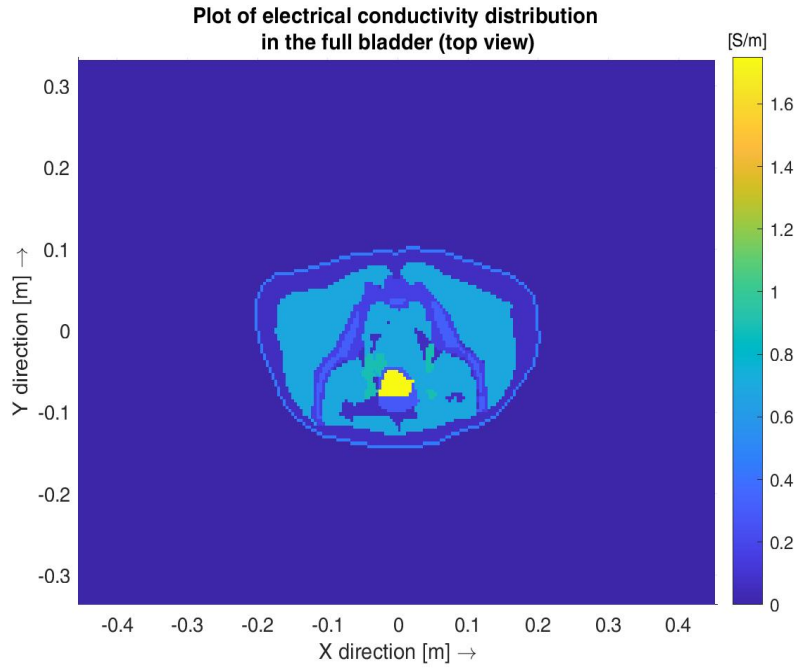
Figure 4.4: Plot of electrical conductivity of the tissues within the chosen cross-section of the Zubal numerical phantom for the case of the full urinary bladder.

However, for further development of the simulator urine was omitted due to its high electrical conductivity value calculated according to the four-pole Cole-Cole model mentioned earlier. High conductivity with respect to other tissues present in the simulated patient torso (see Figure 4.4, region highlighted in bright-yellow color) leads to higher absorption of power by urine and subsequent large value of SAR, which would inevitably create complications during the steering of the antenna elements. Therefore, the empty bladder was modelled. This was done using the knowledge of urinary bladder anatomy. The bladder wall consists of several layers, while the largest part of it is comprised by smooth muscle fibres (the detrusor muscle), which are arranged in a layered manner in three different ways [41]. Therefore, this let conclude that the closest approximation to the urinary bladder wall is the muscle tissue. For the case of the empty bladder, the same mapping of relative permittivity and electrical conductivity is shown in Figures 4.5 and 4.6.

Figure 4.5: Plot of relative permittivity of the tissues within the chosen cross-section of the Zubal numerical phantom for the case of an empty urinary bladder.

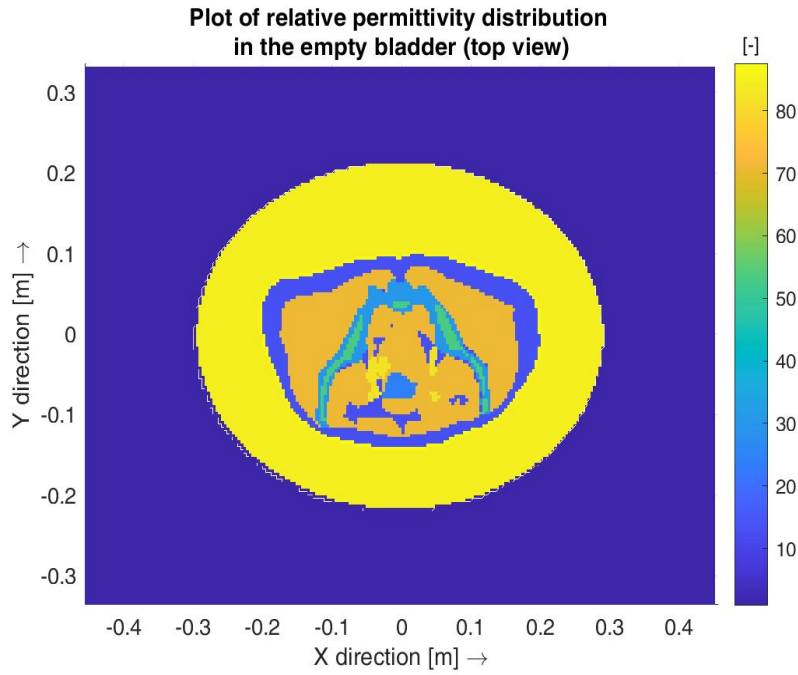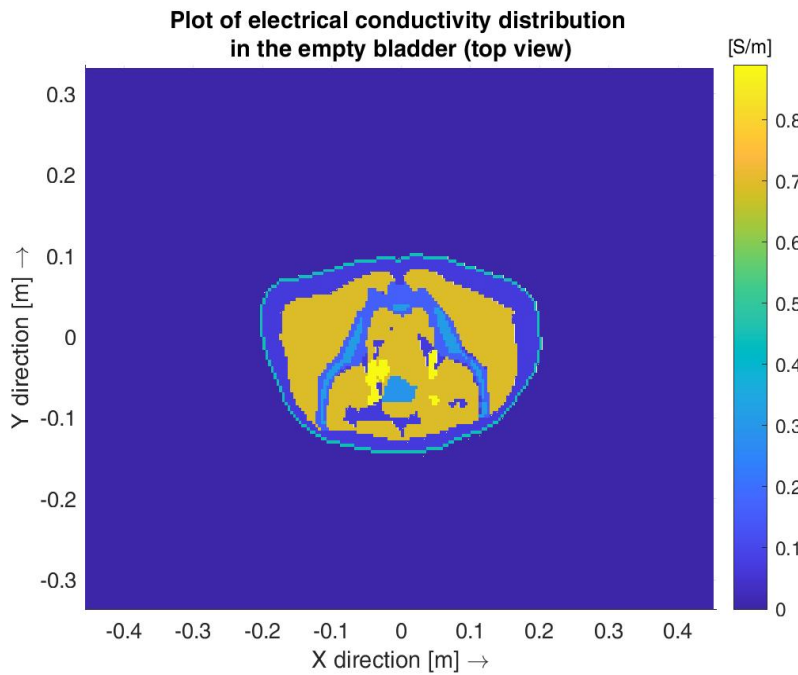Figure 4.6: Plot of electrical conductivity of the tissues within the chosen cross-section of the Zubal numerical phantom for the case of an empty urinary bladder.

After the verification of the correct behaviour of the Cole-Cole model and comparison of the calculated and mapped values of relative permittivity and electrical conductivity to the data in the relevant source [40], the ultimate work with the

FDTD simulator has begun. At first, all four antennas located on the interface of the water bolus and air at four ends of ellipse's semi-axes were turned on. They were chosen to be cylindrical sources and to operate at a frequency of 70 MHz, as this value is widely-used for therapeutic purposes in hyperthermia. Using the pulse with amplitude equal to one and no phase shift, phase vector values were exported from each source as the input data for the subsequent calculation of the total phase vector from all four sources. After exporting, the total phasor value was calculated according to the following equation:

$$E_{z,total} = \sum_{n=1}^{4} E_{z,i} \cdot A_i \cdot e^{\phi_i}, \tag{4.2}$$

where $E_{z,total}$ is the total phase vector from all four sources, $E_{z,i}$ is the exported phasor data from each source for the test pulse, A_i is the amplitude value of the pulse from the respective source, ϕ_i is the phase shift of the pulse from each antenna.

After exporting the phasors, the performance of the simulator was tested for the same two parameters as in the simplified case to ensure the reliability of the developed simulator before moving on to implementing the four beam steering strategies. Three out of four antennas were turned off both in MATLAB and COMSOL simulations, and only the top antenna was left active. Such setting was considered to be sufficient for proper investigation and validation of the performance of the simulator, as in real clinical practice E-fields and SAR are calculated for each antenna separately, therefore, making it possible to carry out the analysis on one antenna only.

The last step in the process was the validation of performance of the created two-dimensional numerical simulator by means of a commercial simulator, namely, COMSOL Multiphysics. The simulator was chosen due to its accuracy, availability for our faculty, flexibility and speedy performance. Taking into account the fact that the model geometry is complex and difficult to recreate in COMSOL Multiphysics manually, the CorelDRAW software was used [42]. CorelDRAW was chosen because one of the file formats exportable from it is compatible with COMSOL, which is not the case with MATLAB.

MATLAB figure containing all tissue indexes with appropriate contrast between the tissues and structures has been imported to CorelDRAW and adjusted for COMSOL Multiphysics. In this case optimisation refers to removing gaps in between tissue structures which could lead to errors during the simulation in COMSOL because by default settings of the algorithm all gaps would be filled with water and bring imbalance to the overall domain geometry. After modification, the edited figure was imported to the existing domain geometry in COMSOL created for the simplified case with two ellipses, which included the air-comprised domain, the water bolus

and four antennas (the ellipse mimicking the muscle tissue was removed because now it was going to get replaced by the realistic anatomy of the patient). The Zubal geometry was rescaled and repositioned to mimic the setting obtained in MATLAB - see figure 4.7. The four sources are positioned in the following figure as follows: source 1 is on the right side of the ellipse (left side of the patient), source 2 is at the bottom of the ellipse (close to the abdomen of the patient), source 3 is on the left side of the ellipse (right side of the patient), and source 4 is at the top (close to the backside of the patient). The next step after the geometric domain adjustment was
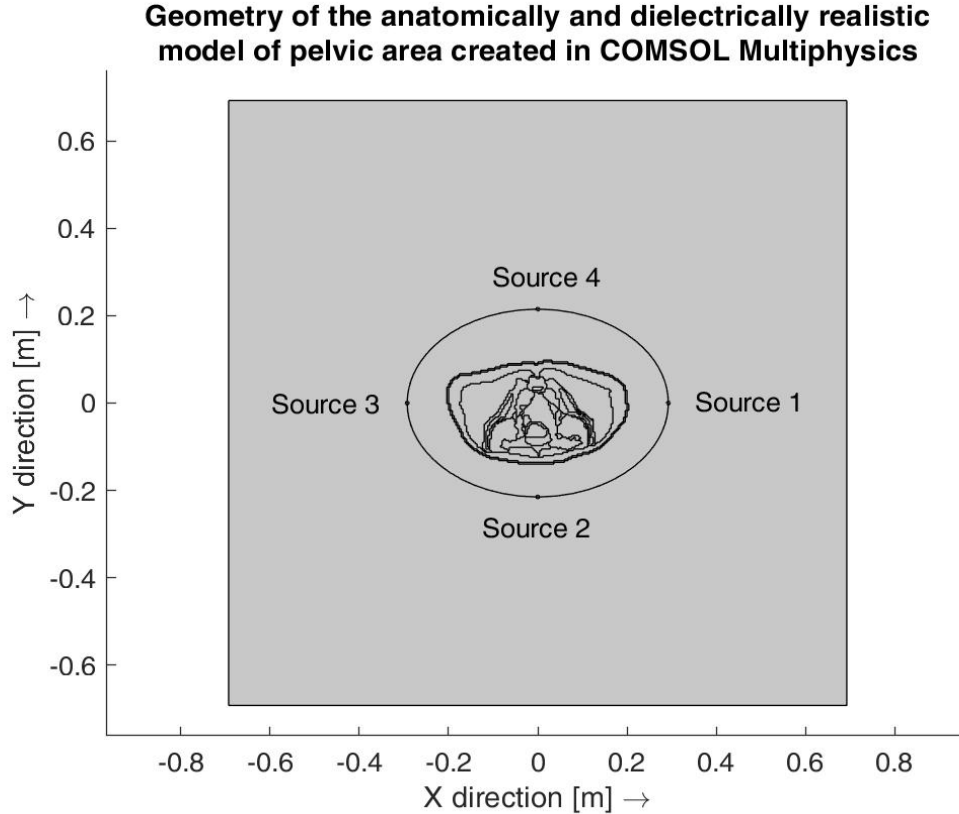
Figure 4.7: COMSOL model geometry for the case of the anatomically and dielectrically realistic model of the pelvic area.

the assignment of relevant dielectric properties taken from the relevant source [40] to all appropriate tissue and organ regions. This step is necessary to simulate the electromagnetic field distribution correctly and make the COMSOL model mimic that from MATLAB. Dielectric properties of all tissues were taken from the same on-line material database [40] as for the MATLAB simulation and entered manually, omitting COMSOL material libraries, although they offer ready sets of relevant dielectric parameters. This was done to guarantee the highest precision within the range of this experiment by decreasing the differences between the two models as much as possible. After assigning the relevant dielectric properties to each tissue, port settings were adjusted to have port input power of the active source equal to $1 \text{ W} \cdot \text{m}^{-1}$, its phase shift equal to 0 radians and setting up scattering boundary

conditions with no incident field and scattered plane wave type of the first order, s
in the previous case with the simplified model of the pelvic area. This was the last
step in preparing the model in COMSOL Multiphysics at this point of simulator
development. Next steps are devoted to the implementation of the four mentioned
beam steering strategies.

4.3 THQ driven global optimization

The first beam steering strategy was THQ driven global optimization. The main
task of the THQ function is to find such values for amplitudes and phases of the
sources so as to minimise the effect of hotspots on the quality of therapy. THQ
(Target to Hot-Spot Quotient) is defined as shown in equation

$$THQ = \frac{<SAR_{target}>}{<SAR_{HS}>} \tag{4.3}$$

where $<SAR_{target}>$ is the mean SAR in the target volume and $<SAR_{HS}>$ is the
average SAR in hotspots, defined as the 1% volume of healthy tissue volume where
the highest SAR occurs [43]. Since most of optimisation algorithms implemented in
MATLAB are designed in a way to find the minimum of the function, the minimised
THQ (or HTQ) was used.

The next step was the calculation of the total E-field phasor as a linear combina-
tion of individual phasors, given the exported data from all four sources, according
to equation 4.2. It was followed by the calculation of SAR in the entire model and
determination of the minimum and maximum value of this parameter in the entire
computational domain. The next step is of great importance and is connected with
a choice of a mask. Mask is a tool separating the target and healthy tissue. Masks
come in a great variety of shapes and forms, depending on the purpose of the appli-
cation. For the case of this thesis, circular mask of a target was chosen. Apart from
the target itself, healthy tissue also has a mask which corresponds to the remaining
part of the patient model geometry.

Having chosen the mask type, the average SAR in the target was calculated as
the sum of the SAR in the target divided by the area of the target (or the mask).
Next, the mask for healthy tissue was created as a simple difference of the entire
domain and the mask of the target. Finally, the SAR in healthy tissue was ob-
tained, which was used to calculate the mean value of this parameter in 1 % of
the hotspot. Then, the THQ itself was found as the ratio of the mean SAR in
1 % of the hotspot and the mean SAR in the target. In this thesis, minimised
THQ was evaluated, meaning the minimisation of the ratio of the mean SAR in 1
% of the hotspot and the mean SAR in the target was performed via PSO. The

full algorithm for the evaluation of the criteria function is available within the file attachment "criterial_function_THQ.m". The limitation that stems at this point is that the criteria function needs to be evaluated every time the optimization process is run. Therefore, in clinical practice it is common to use GPU for accelerating the evaluation of criteria function and subsequent PSO (Particle Swarm Optimisation). PSO technique was chosen because it has the ability to escape from local minima of the function of interest (THQ in this thesis) and it strives to reach the real global minimum instead, however, it can never end up there. Instead, it will remain close to the global minimum. Reaching the global minimum was ensured by the implementation of a deterministic algorithm following PSO optimisation, which looked for the minimum of constrained nonlinear multivariable function (MATLAB syntax *fmincon*).

Having mentioned PSO, it works on a principle of the use of the parameters found in the previous step as inputs with some additional features. Namely, these are the lower and upper bounds of the values and options that are available to be specified within MATLAB. For the case of this thesis, the number of iterations of the algorithm, function tolerance, display of results and swarm size were set as optional features. With the use of exported E-fields from all sources individually, maps of electrical conductivity, density and index distribution within the computational domain, it was possible to again calculate the total E-field phasor and SAR, together with the maximum value for the latter. Finally, given the number of spatial steps in both x and y directions as references regarding the axes, the new optimised SAR distribution was plotted. The full optimisation algorithm can be found within the attachment to this thesis under the name "Optimisation_THQ.m".

4.4   Generalized Eigenvalue Approach

Generalized Eigenvalue Approach is a mathematically elegant approach designed to focus the energy on the target (tumor region). The first step in its creation is similar to that of THQ - the masks of target and healthy tissue region have to be created. Masks can be circular, elliptical or region-specific (mimicking the outlines of a particular organ). In this thesis, circular masks were used.

The problem that the Generalized Eigenvalue Approach is meant to solve can mathematically be described as follows:

$$\max_{p \in \mathbb{C}^N, \|p\|} \frac{\int_{\Omega \sigma(x)} |\overrightarrow{\underline{E}}(p,x)^2| \, dV}{\int_{G \setminus \Omega} \sigma(x) |\overrightarrow{\underline{E}}(p,x)^2| \, dV}, \tag{4.4}$$

42

where Ω is the area where the energy has to be focused (tumour tissue) and $G \setminus \Omega$ is the healthy tissue. $\sigma(x)$ is the electrical conductivity of tissues in the selected region, $\overrightarrow{\underline{E}}$ is the phasor of the E-field vector and dV is the elementary integration volume. The main aim of the method is to maximize the fraction by finding the vector p including the complex amplitudes of antenna signals.

(4.4) can be rewritten in the following form:

$$\max_{p \in \mathbb{C}^N, \|p\|=1} \frac{\langle p, A\overline{p} \rangle \mathbb{C}^N}{\langle p, B\overline{p} \rangle \mathbb{C}^N}, \tag{4.5}$$

where matrices A and B are defined as

$$A_{ij} = \int_{\Omega} \sigma(x) \overrightarrow{\underline{E}}_i(x) \overline{\underline{E}_j(x)} dx \tag{4.6}$$

$$B_{ij} = \int_{G \setminus \Omega} \sigma(x) \overrightarrow{\underline{E}}_i(x) \overline{\underline{E}_j(x)} dx \tag{4.7}$$

If equation 4.5 is set to $\lambda, it can be written that \frac{pA\overline{p}}{pB\overline{p}} = \lambda (4.8)$ then

$$A\overline{p} = \lambda B\overline{p}. \tag{4.9}$$

If for a square matrix A (N × N), a non-zero vector v (N × 1) and a scalar number λ holds

$$Av = \lambda v, \tag{4.10}$$

the vector v is called the eigenvector and the scalar λ the eigenvalue of matrix A.

As regards the implementation in MATLAB, after calculating elements of matrices A and B according to equations 4.6 and 4.7, two square matrices (4 × 4) were obtained because four sources were used in the simulation. Then, using the MATLAB command *eig* a diagonal matrix with eigenvalues of the matrix B and a matrix with corresponding eigenvectors were obtained. From the set of calculated eigenvalues, a maximum result was chosen and the eigenvector corresponding to it was identified. From this vector, the optimized amplitudes and phases of all four sources were determined. They were then used for the calculation of the total phasor of the electromagnetic resulting from the activity of all antenna elements using equation 4.2. The last steps were the calculation of SAR in the computational domain after optimization using the total phasor of the electromagnetic field and evaluation of treatment planning quality [44].

4.5 Time-Reversal

The following focusing technique has been chosen for investigation due to emerging success of methods based on time-reversal. It has the advantage of being patient specific and can be used in both pulsed wave and continuous applications. Another advantageous difference is the estimation of phases and amplitudes of antennas from simulation of wave transmission and not from measured data. This approach allows for placing the point source in defined focus points in the tumor in case when multiple focus points are required. This allows instantaneous sweeping of the focusing points during the treatment, which can be useful in case of complex tumor geometries.

The general approach towards the implementation of this technique, which was used in this thesis, is as follows. At first, the wave propagates from the source through the patient model from a virtual antenna placed in the tumor. This virtual point source was excited with a sinusoidal signal with a frequency 70 MHz. The point source was placed in the center of the tumor, as this location is considered the most optimal choice. Then, the simulated radiated field is "sensed" at the locations of the antenna elements. The real antenna system is then transmitting the field in a time-reversed order, meaning from $t = T$ to $t = 0$, where T is the time when the simulated signal from the virtual point source vanishes. The invariance of the wave equation under time-reversal in lossless media enables to perform approximate focusing of time-reversed signal at the original source even in lossy media [45].
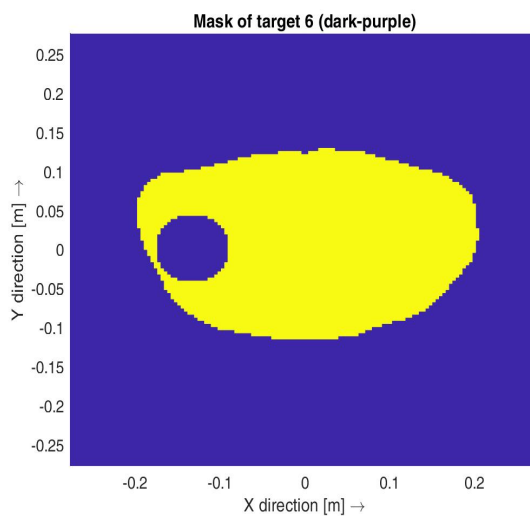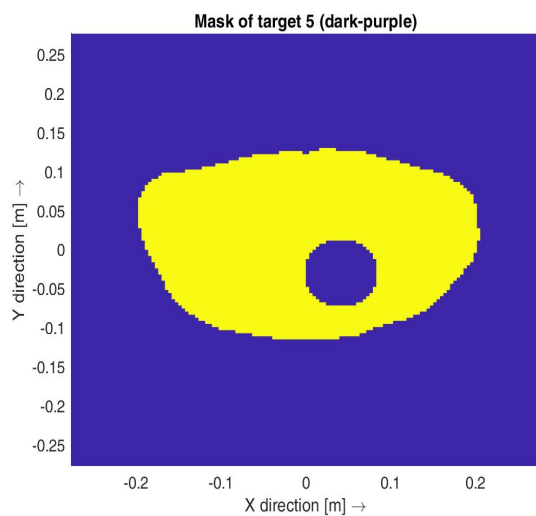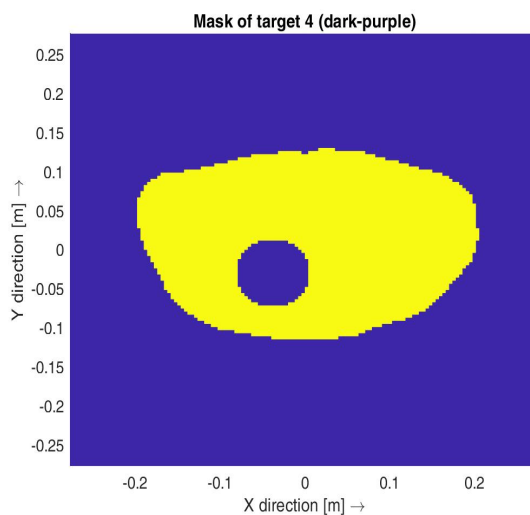
4.6 Target Centre Point (TCP) steering

Target Centre Point method was chosen because its approach towards optimisation differs from that of the three methods presented before. Mainly, the difference lies in the fact that TCP enables to quickly calculate the phases of antenna elements without requiring treatment planning. Its core principle is that a homogeneous patient model consisting of muscle tissue is created and for each antenna phase delays are calculated analytically using the difference in phase shift in muscle tissue and water. These phase shifts are calculated in such a way that the maximum interference would occur at the desired target centre point within the elliptical phantom. These phases with reversed signs are then used in the setup of the real hyperthermia system which operates on real patient anatomy. The amplitudes of all antennas are always considered to be equal [46].

4.7 Further study of treatment planning algorithms

After the implementation of all four beam steering strategies in MATLAB, it was necessary to evaluate the treatment planning quality for each of them. It was done

in MATLAB using 10 different target locations via the implementation of the two parameters used for this purpose - TC25 and TC50. TC25 and TC50 are used in clinics as indicators of how much (in %) of the tumor volume is covered with SAR that is higher than either 25% or 50% of the maximal SAR in the entire computational domain.

10 target locations were chosen to have circular shapes for better compatibility with domain geometry. Another shape of targets that is often used is elliptical or region-specific, where the target contours follow the outlines specified by the physician. The radius of the targets was chosen to be 87.3 mm which is the mean value of lengths of the semi-axes of the ellipse used as a target mask in real clinical practice (personal consultation with Ing. Tomáš Dříž'al, Ph.D., on 04.04.2022). The targets were located in different positions of the patient model to provide various settings for the accurate evaluation of treatment planning quality of all four beam steering strategies - see figure 4.8. This evaluation was performed both qualitatively and quantitatively. In the first case the analysis was performed in terms of assessing the SAR distribution for each target. In the latter case, values of computed TC25 and TC50 parameters were considered.

Mask of target 1 (dark-purple)

Mask of target 2 (dark-purple)

Mask of target 3 (dark-purple)

Mask of target 4 (dark-purple)

Mask of target 5 (dark-purple)

Mask of target 6 (dark-purple)
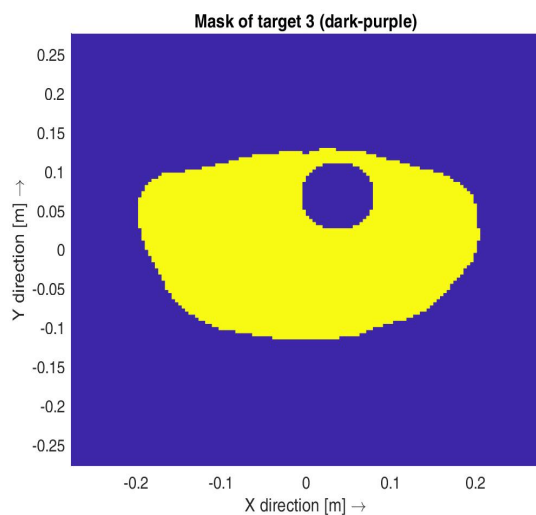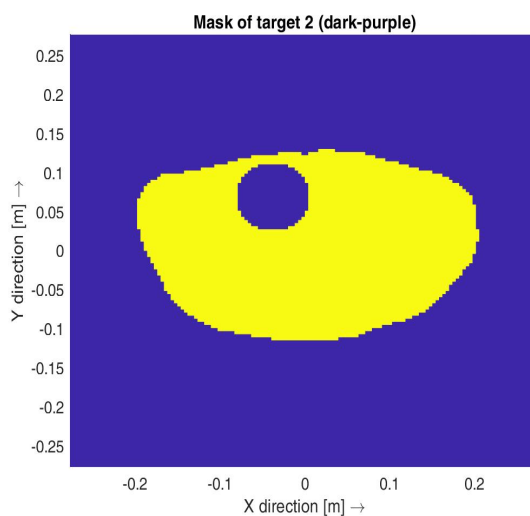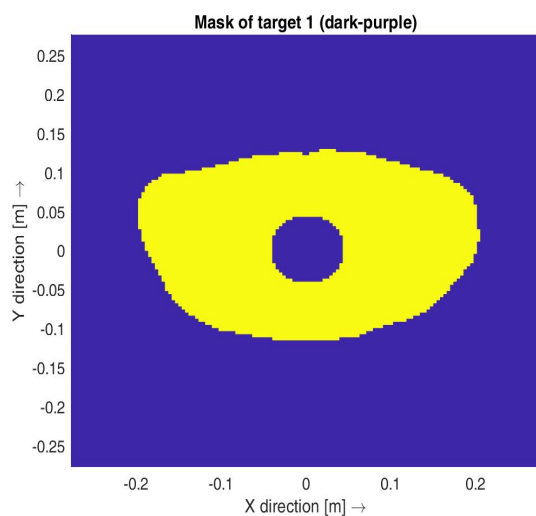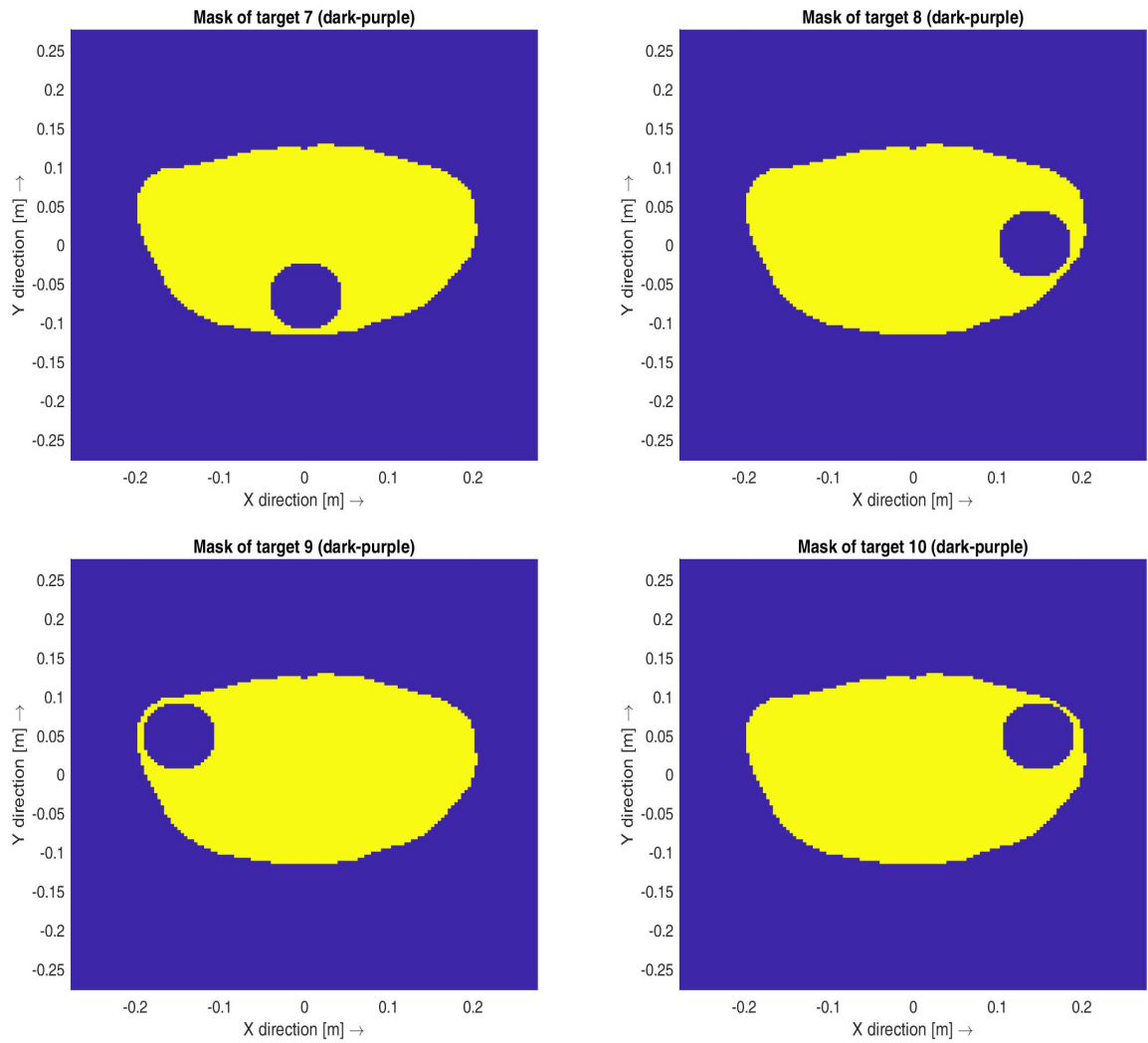
Figure 4.8: 10 target locations within the patient model.

5 Results

5.1 Development of 2D FDTD-based simulator for a simplified model of pelvic area

After completing the development of the simplified simulator for the case of the elliptical model, its performance was visualized for two parameters of interest within this work – E-field distribution and SAR distribution, both normalised. As it was previously mentioned in the *Methods* section, the creation of a simulator in MATLAB was followed by the creation of the corresponding model in COMSOL Multiphysics. After the model was created, the same parameters as those evaluated in MATLAB were plotted for comparing the similarity of performance of both simulations and thus for confirming the validity of results obtained from the developed FDTD-based simulator. The results obtained for all these parameters are shown in Figures 5.1 - 5.4.

Figure 5.1: Magnitude of the E-field phasor in a simplified patient model obtained from the FDTD-based simulator in MATLAB. *Normalised and thus unit-less.* Source 4 is active.

Figure 5.2: Magnitude of the E-field phasor in a simplified patient model obtained from COMSOL Multiphysics. *Normalised and thus unit-less.* Source 4 is active.
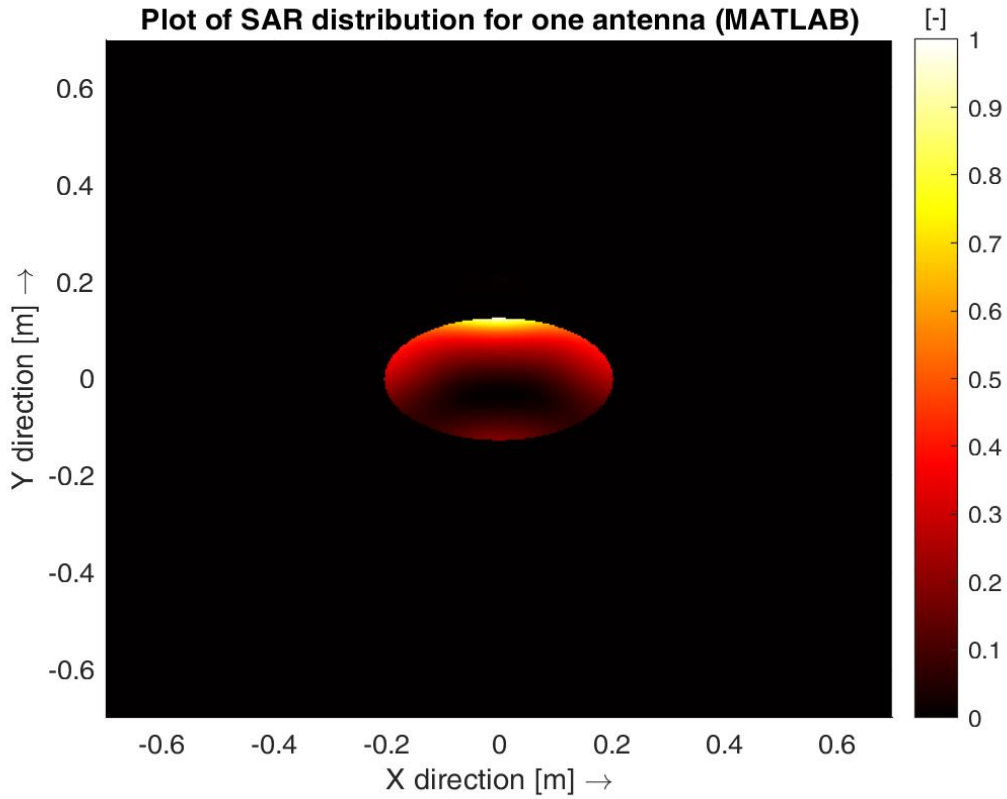
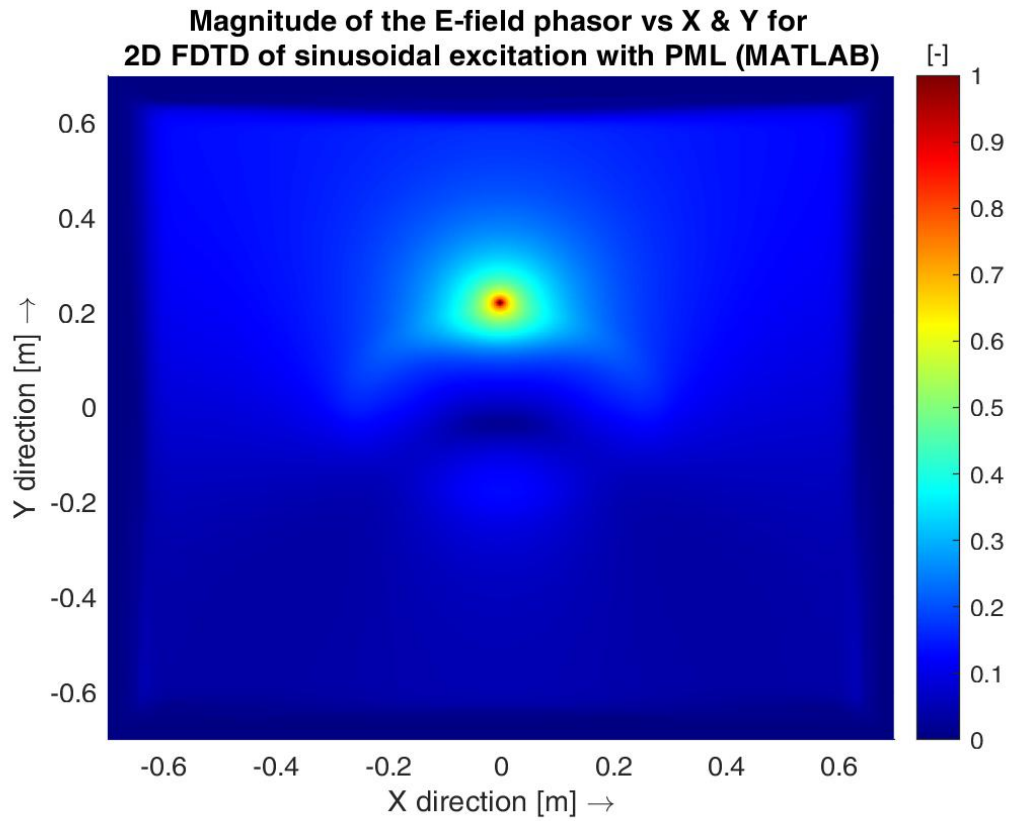Figure 5.3: Distribution of SAR in a simplified patient model obtained from the FDTD-based simulator in MATLAB. *Normalised and thus unit-less.* Source 4 is active.
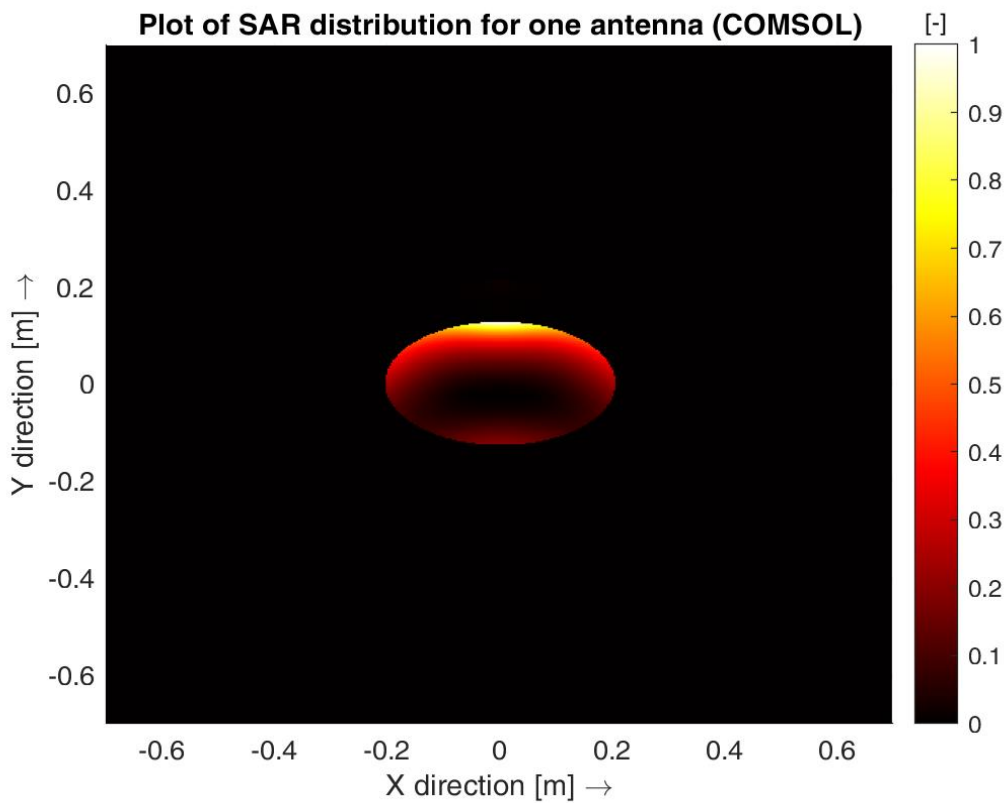
Figure 5.4: Distribution of SAR in a simplified patient model obtained from COMSOL Multiphysics. *Normalised and thus unit-less.* Source 4 is active.

5.2 Development of 2D FDTD-based simulator for anatomically and dielectrically realistic model of pelvic area

After the simplified simulator was developed and tested in both MATLAB and COMSOL Multiphysics, it was upgraded to perform on an anatomically and dielectrically realistic model of a human pelvic region. After the completion of necessary modifications in MATLAB, its performance was visualized for two main parameters of interest within the scope of this thesis - E-field distribution and SAR distribution, both normalised. The same parameters were extracted from the created corresponding COMSOL Multiphysics simulation model for analysing the performance and validity of the developed complex numerical simulator. These parameters are shown in Figures 5.5 - 5.8.
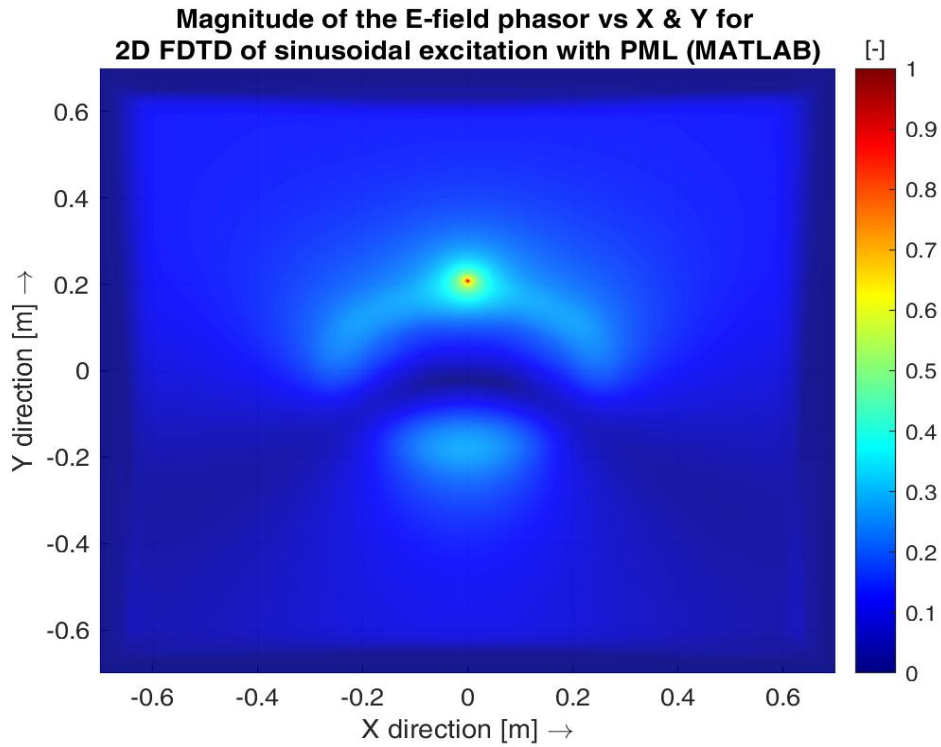
Figure 5.5: Magnitude of the E-field phasor in anatomically and dielectrically realistic patient model obtained from the FDTD-based simulator in MATLAB. *Normalised and thus unit-less.* Source 4 is active.
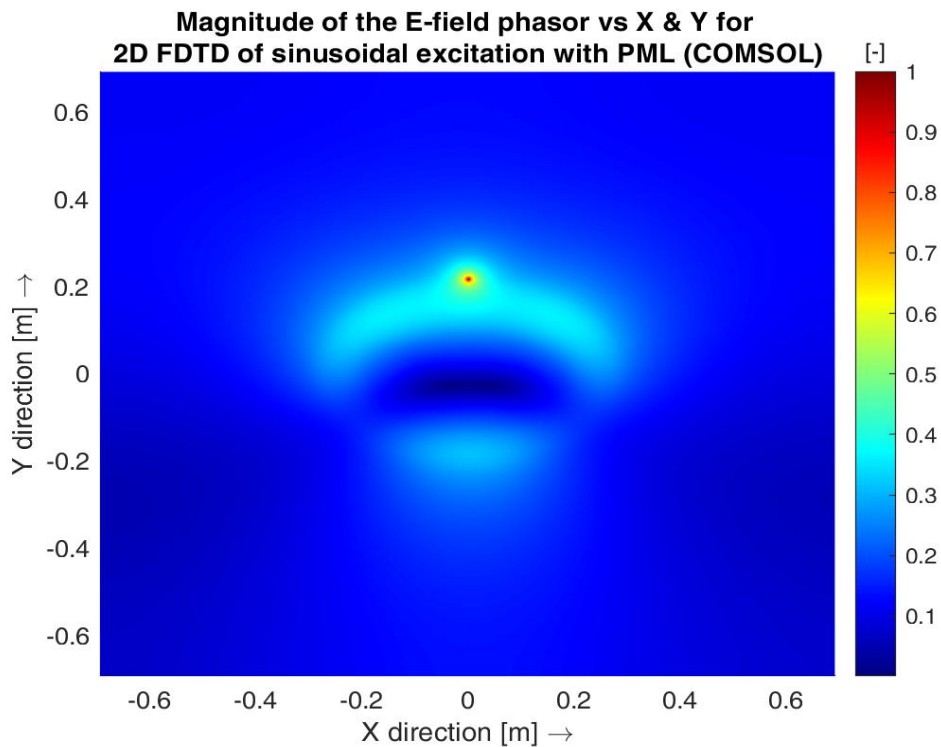
Figure 5.6: Magnitude of the E-field phasor in anatomically and dielectrically realistic patient model obtained from COMSOL Multiphysics. *Normalised and thus unit-less.* Source 4 is active.
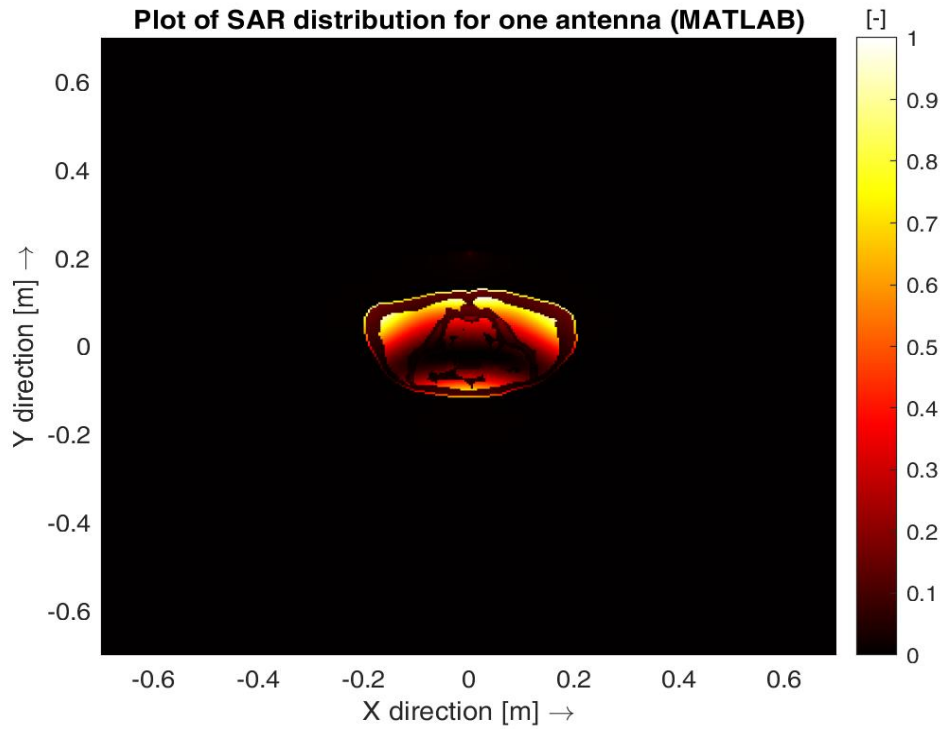
Figure 5.7: Distribution of SAR in anatomically and dielectrically realistic patient model obtained from the FDTD-based simulator in MATLAB. *Normalised and thus unit-less.* Source 4 is active.
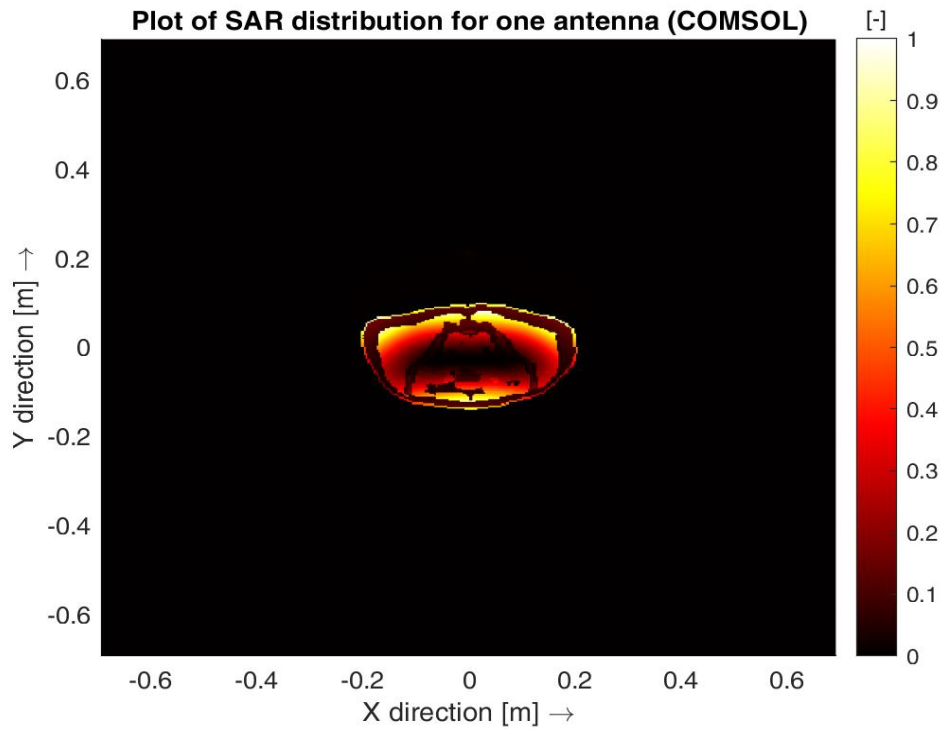
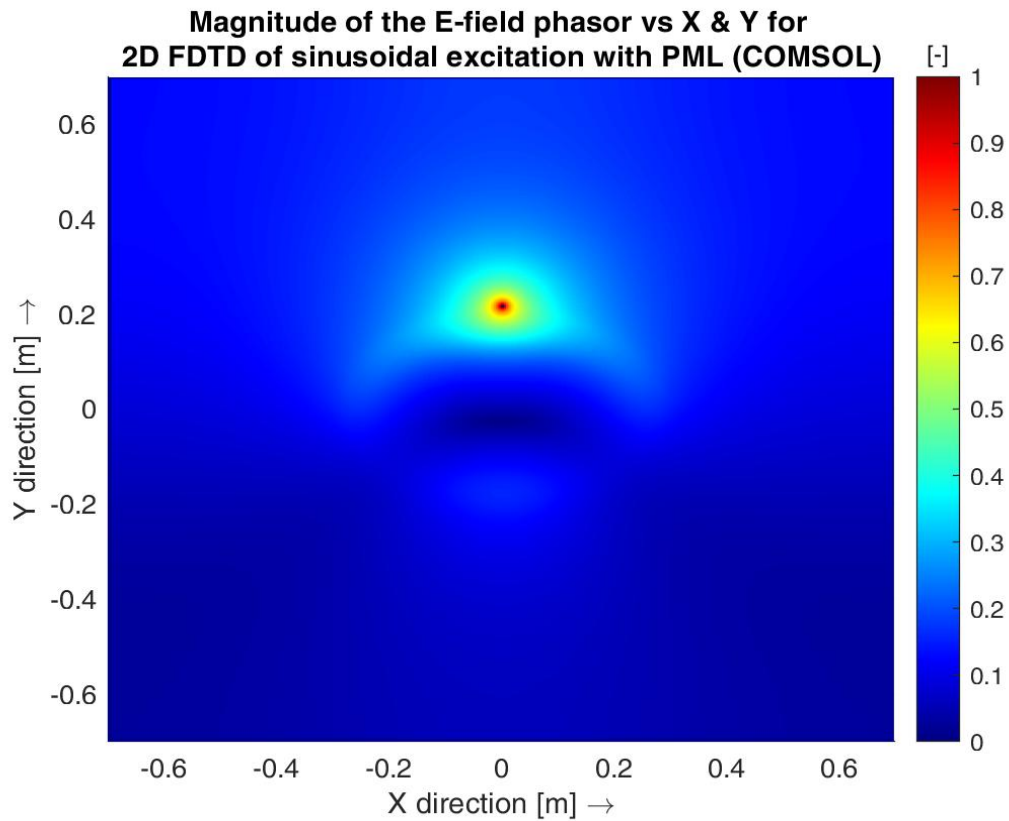Figure 5.8: Distribution of SAR in anatomically and dielectrically realistic patient model obtained from COMSOL Multiphysics. *Normalised and thus unit-less.* Source 4 is active.

## 5.3 Results of implementing beam steering strategies

This sub-chapter contains the results of implementation of four beam steering strategies - THQ driven global optimization, generalized eigenvalue approach, time-reversal and target centre point steering. As a parameter for qualitative evaluation of the above-mentioned algorithms, the optimised SAR distribution for all 10 targets is shown in figures 5.9 - 5.13. Quantitative evaluation is based on the calculated values of TC25 and TC50 parameters as well as the value of the THQ cost function for each target, all of which are presented in tables 5.1 and 5.2, respectively. Tables 5.3 - 5.6 show the values of optimized amplitudes and phases of all sources for each treatment planning algorithm and every target.

TC25 [%]				
Target number	THQ driven global op-timization	Generalized Eigenvalue Approach	Time-reversal	Target centre point steering
1	91.2	80.4	72.4	80.4
2	57.6	0.0	59.5	57.6
3	57.1	0.0	59.5	57.1
4	65.7	0.0	57.9	63.3
5	85.3	0.0	13.1	83.4
6	77.7	83.1	0.0	68.9
7	55.0	0.0	15.8	50.7
8	64.6	75.6	0.0	59.8
9	61.1	61.1	15.6	61.1
10	58.4	58.5	0.0	54.4
Average [%]	67.4	35.9	29.4	63.7
Standard deviation [%]	12.8	38.6	29.3	10.8
TC50 [%]				
1	80.4	0.3	6.4	9.1
2	32.4	0.0	50.9	8.9
3	33.8	0.0	26.8	21.7
4	36.3	0.0	7.2	2.2
5	61.1	0.0	0.0	21.5
6	45.6	80.4	0.0	37.0
7	39.9	0.0	0.0	0.0
8	23.9	71.9	0.0	28.4
9	56.6	61.1	0.0	32.7
10	47.7	58.5	0.0	24.4
Average [%]	45.8	27.2	9.1	18.6
Standard deviation [%]	16.6	35.6	16.9	12.8

Table 5.1: Evaluated TC25 and TC50 parameters for 10 targets after source optimisation by four investigated algorithms, their average and standard deviation.

Target number	Best value of THQ cost function	THQ value for generalized eigenvalue approach	THQ value for time-reversal	THQ value for TCP
1	0.99	0.68	0.51	0.83
2	1.52	0.06	0.97	0.59
3	1.46	0.05	0.59	0.60
4	0.82	0.28	0.43	0.62
5	1.21	0.29	0.24	0.73
6	3.02	1.44	0.13	1.83
7	1.50	0.10	0.27	0.49
8	3.18	1.15	0.03	1.70
9	2.42	0.97	0.22	1.27
10	1.85	0.90	0.06	1.11

Table 5.2: Values of THQ for source optimization for the case of each target.

Optimized amplitudes (normalized) [-]				
Target number	Source 1 (right)	Source 2 (bottom)	Source 3 (left)	Source 4 (top)
1	0.93	0.61	1.00	0.47
2	1.00	0.66	0.39	0.47
3	1.00	0.62	0.30	0.67
4	0.55	0.62	1.00	0.62
5	0.51	0.74	1.00	0.54
6	0.58	0.88	0.51	1.00
7	0.09	0.59	1.00	0.56
8	0.38	1.00	0.30	0.94
9	1.00	0.90	0.90	0.85
10	1.00	0.73	0.59	0.83
Signal phase shift [rad]				
1	6.04	0.32	0.00	6.28
2	5.42	6.20	0.94	0.08
3	2.52	3.51	3.61	2.92
4	0.23	6.28	0.00	0.45
5	6.10	0.15	5.40	5.64
6	5.60	1.40	5.61	0.44
7	3.89	3.15	2.54	2.96
8	5.57	0.35	5.85	1.15
9	2.43	0.54	5.08	5.56
10	3.22	6.28	0.00	1.35

Table 5.3: Optimized amplitudes and phases for all sources and targets by THQ driven global optimization.

Optimized amplitudes (normalized) [-]				
Target number	Source 1 (right)	Source 2 (bottom)	Source 3 (left)	Source 4 (top)
1	1.00	0.26	0.98	0.39
2	0.59	0.75	1.00	0.98
3	1.00	0.75	0.56	1.00
4	0.60	0.62	1.00	0.10
5	1.00	0.64	0.55	0.14
6	0.44	0.96	1.00	0.87
7	1.00	0.88	0.92	0.79
8	0.98	1.00	0.43	0.90
9	0.38	0.59	0.91	1.00
10	0.89	0.61	0.35	1.00
Signal phase shift [rad]				
1	0.00	1.21	0.00	1.97
2	-0.44	-2.52	0.0	1.68
3	0.00	-2.58	-0.49	1.70
4	-0.68	0.92	0.00	-2.82
5	0.00	0.92	-0.74	-2.87
6	2.66	-0.74	0.00	-0.65
7	0.00	1.64	0.00	-2.48
8	0.93	0.00	-2.98	0.08
9	2.92	-0.69	0.51	0.00
10	0.54	-0.68	2.94	0.00

Table 5.4: Optimized amplitudes and phases for all sources and targets by generalized eigenvalue approach.

Optimized amplitudes (normalized) [-]				
Target number	Source 1 (right)	Source 2 (bottom)	Source 3 (left)	Source 4 (top)
1	0.55	0.42	1.00	0.39
2	0.82	0.74	1.00	0.39
3	0.47	0.59	1.00	0.29
4	0.71	0.36	1.00	0.49
5	0.37	0.31	1.00	0.35
6	1.00	0.43	0.51	0.52
7	0.42	0.21	1.00	0.37
8	0.22	0.42	1.00	0.31
9	1.00	0.61	0.48	0.46
10	0.23	0.50	1.00	0.29
Signal phase shift [rad]				
1	1.26	0.00	1.21	1.51
2	1.40	0.00	1.58	1.87
3	1.48	0.00	1.26	1.76
4	1.09	0.00	1.31	1.40
5	1.18	0.00	0.82	1.23
6	1.25	0.00	2.04	1.83
7	0.88	0.00	0.69	0.98
8	1.56	0.00	0.72	1.36
9	1.35	0.00	2.11	1.98
10	1.35	0.00	2.11	1.98

Table 5.5: Optimized amplitudes and phases for all sources and targets by time-reversal.

Optimized amplitudes (normalized) [-]				
Target number	Source 1 (right)	Source 2 (bottom)	Source 3 (left)	Source 4 (top)
1	1.00	1.00	1.00	1.00
2	1.00	1.00	1.00	1.00
3	1.00	1.00	1.00	1.00
4	1.00	1.00	1.00	1.00
5	1.00	1.00	1.00	1.00
6	1.00	1.00	1.00	1.00
7	1.00	1.00	1.00	1.00
8	1.00	1.00	1.00	1.00
9	1.00	1.00	1.00	1.00
10	1.00	1.00	1.00	1.00
Signal phase shift [rad]				
1	1.24	0.00	1.24	0.00
2	3.08	2.30	1.93	0.00
3	1.82	2.25	3.09	0.00
4	2.29	0.00	1.09	0.98
5	1.01	0.00	2.34	0.97
6	4.37	1.81	0.00	1.71
7	2.39	0.00	2.39	2.02
8	0.00	2.25	4.90	2.16
9	4.67	2.56	0.00	1.37
10	0.00	2.65	4.79	1.48

Table 5.6: Optimized amplitudes and phases for all sources and targets by TCP method.

Figure 5.9: SAR distribution optimised by four different algorithms for targets 1 and 2.

Figure 5.10: SAR distribution optimised by four different algorithms for targets 3 and 4.

Figure 5.11: SAR distribution optimised by four different algorithms for targets 5 and 6.
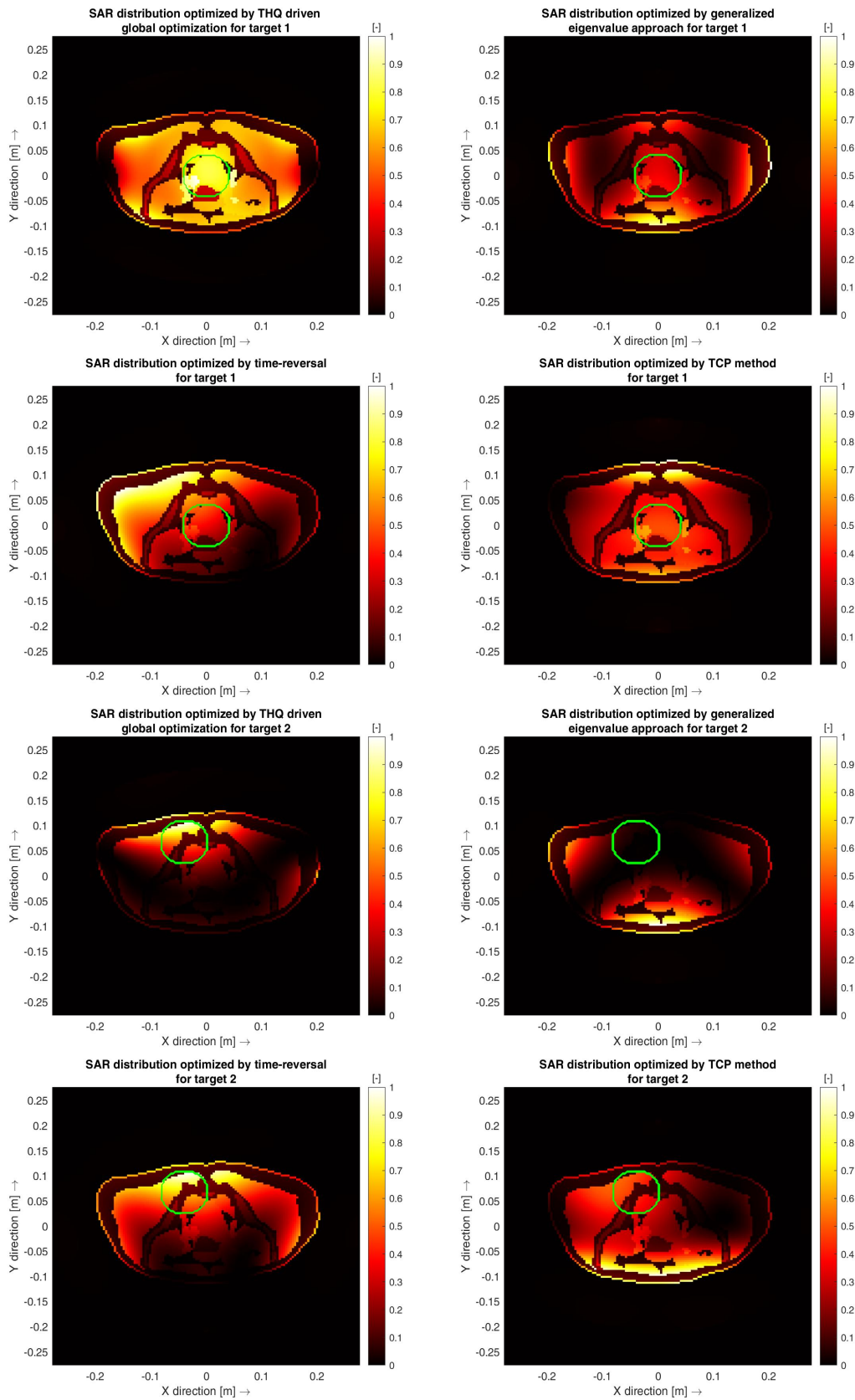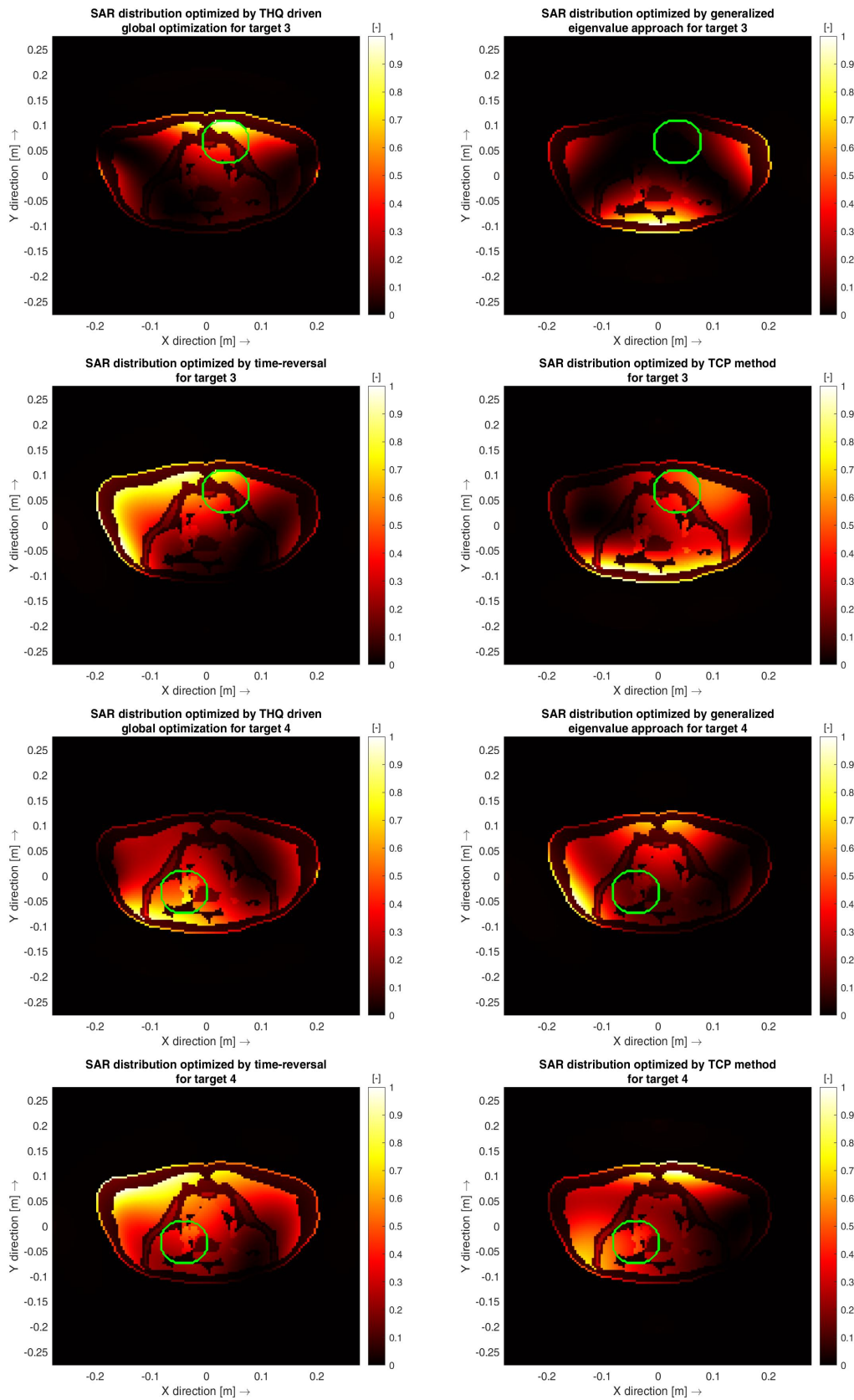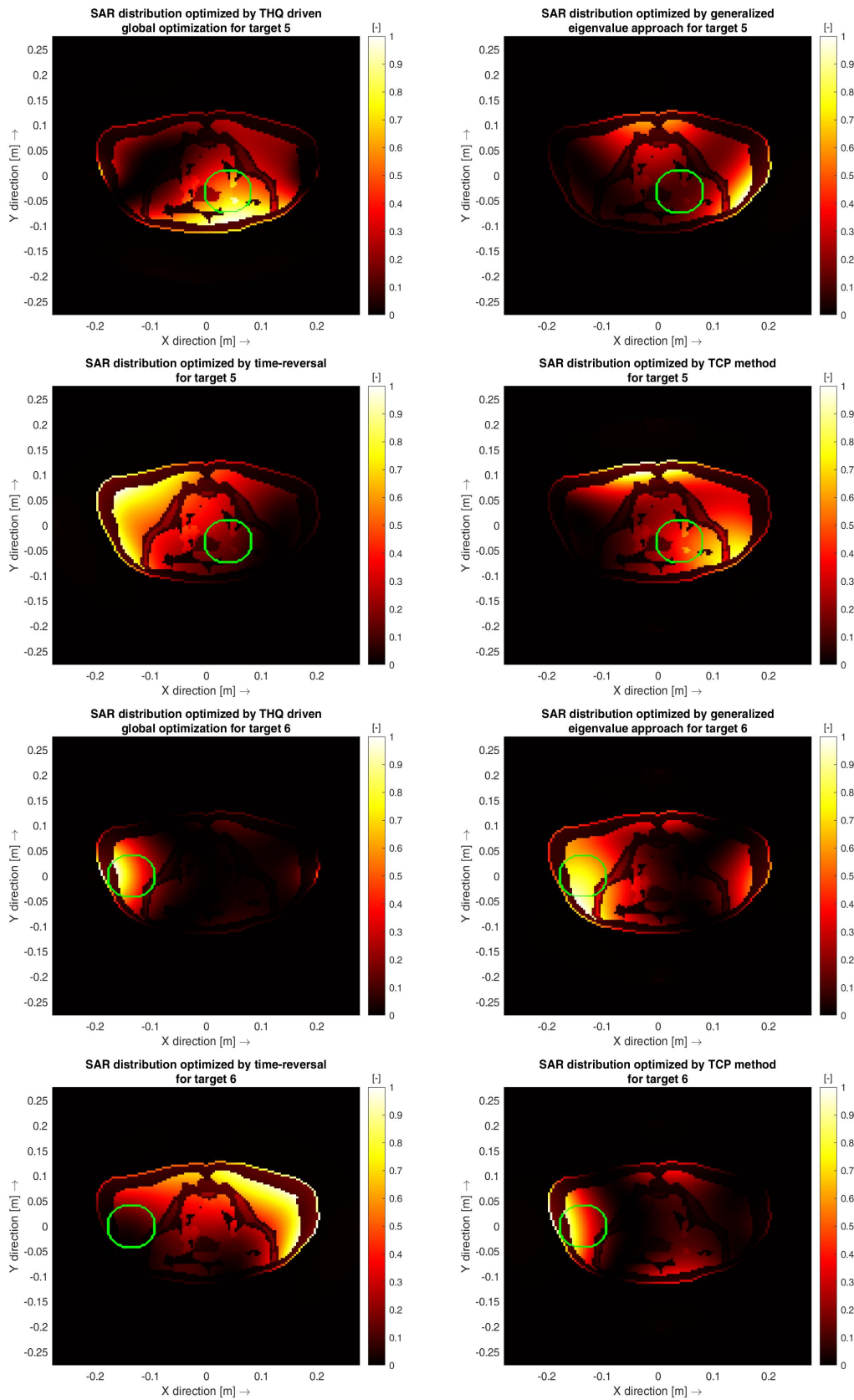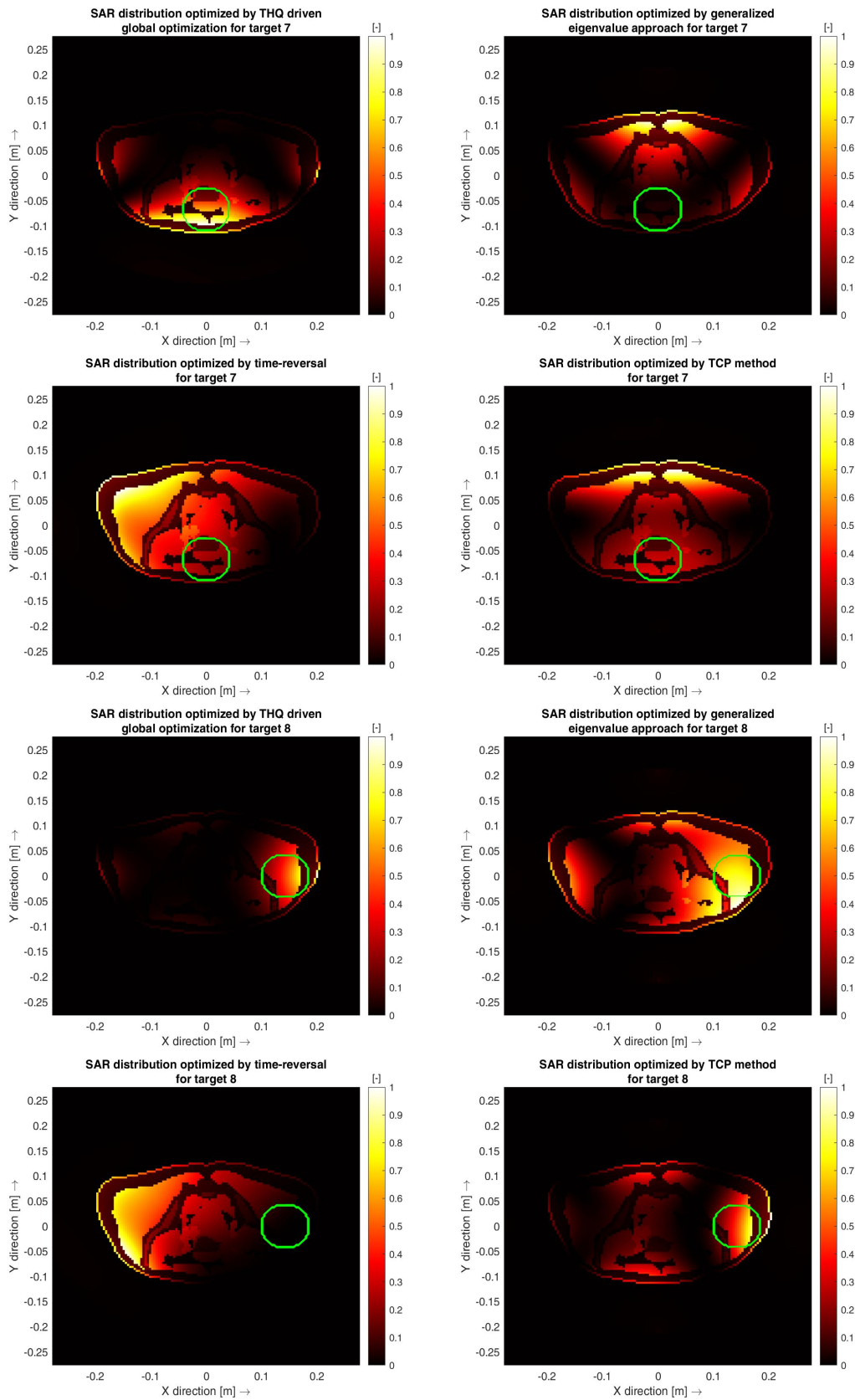
Figure 5.12: SAR distribution optimised by four different algorithms for targets 7 and 8.
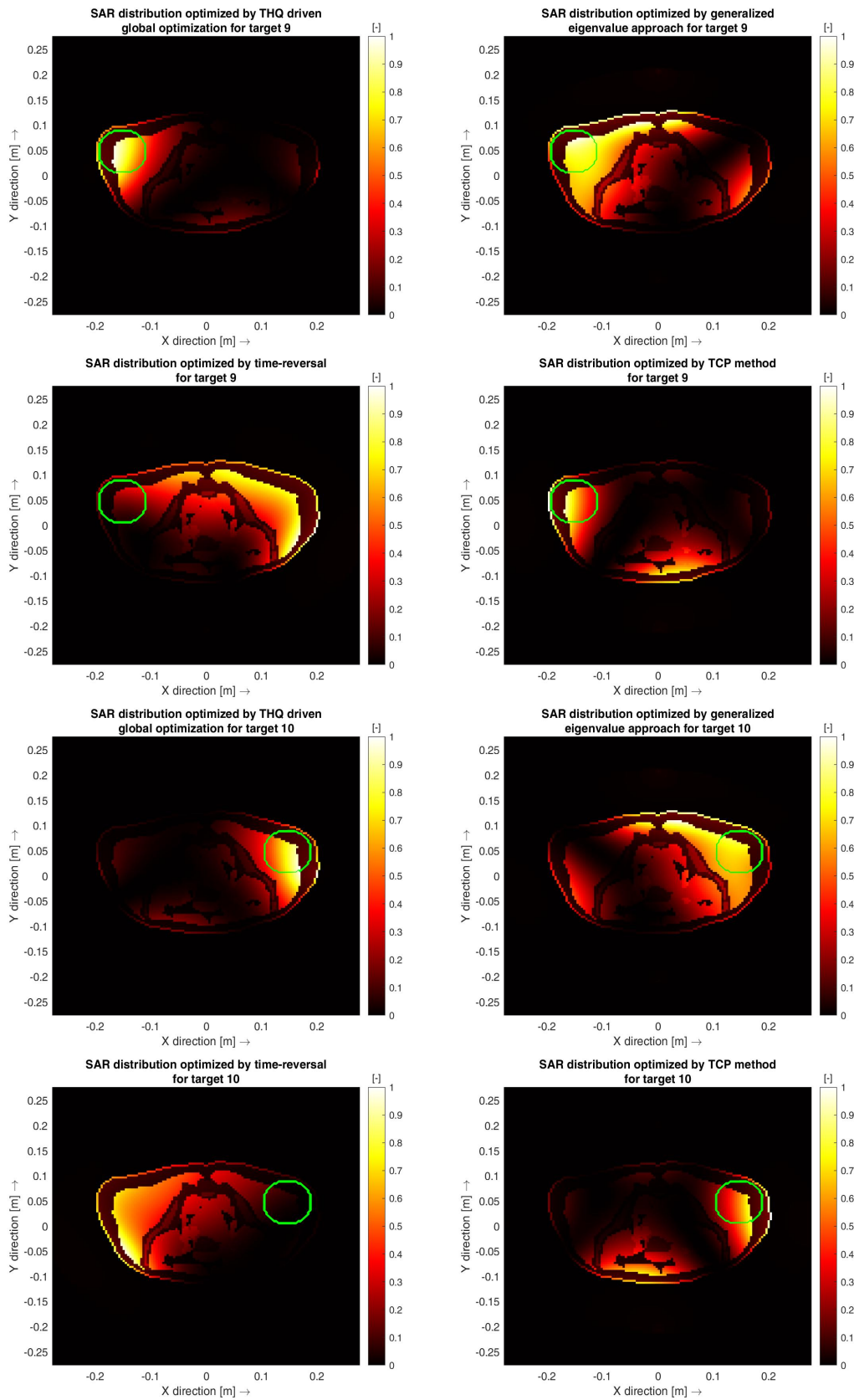
Figure 5.13: SAR distribution optimised by four different algorithms for targets 9 and 10.

6 Discussion

6.1 Analysis of performance of the 2D FDTD-based simulator on a simplified model of pelvic area

The created simulator shows true-to-life properties which proves that it can be considered an accurate tool as regards simulating the distribution of the main investigated parameters - electric field and SAR.

Speaking about the initial simplified case of simulator development, one can, at first, notice the realistic behaviour of the simulator. By looking at figure 5.1 it is evident that the value of the normalised E-field phasor is highest at the position of the source and then gradually decreases as the wave propagates into the water bolus and patient model. In the proximity of the source, the E-field moves sideways from the source with the direction of propagation resembling an outline of the ellipse. This results from the geometry and dielectric properties of the water bolus along and through which the surface wave propagates.

Regarding comparison of FDTD and COMSOL outputs, one can notice a clear correspondence between the results obtained from both software regarding the distribution of the electric field. The interpretation of figures 5.1 and 5.2 lets conclude that the greatest amplitude of the electric field was observed at the location of the source in both simulations. Since the E-field phasor is dependent on the setting of the amplitude and phase of the antennas, the results obtained from both MATLAB and COMSOL Multiphysics were normalised for the ease of analysis and comparison of results of both simulations. Phase setting was omitted in the investigated simulations since for one active antenna it is irrelevant to introduce the phase shift. Otherwise, the amplitude of the electric field phasor was lowering in both directions of wave propagation – away from the source into the air and into the patient. This result confirmed the real behaviour of the system because the expectation was that the muscular layer, due to moderate conductivity, would attenuate the wave to a certain degree - therefore, lowering its amplitude. Similar tendency in the propagation of the E-field is valid for air, there the decrease of amplitude corresponds to cylindrical spreading of the induced waves.

Speaking about SAR distribution, it is again possible to notice an agreement between the results obtained from MATLAB and COMSOL Multiphysics. Figures 5.3 and 5.4 both confirm the expected behaviour of this parameter. Since the body surface (typically, skin, but at this point the outermost layer of the muscle-comprised ellipse) is the first type of biological tissue that comes in contact with the energy radiated from the antenna, it was expected that this outermost layer would be heated up the most and, therefore, have the greatest value of SAR. As the wave

propagates further and deeper into the body, its amplitude decreases due to a number of factors (e.g. attenuation by tissues), and the value of SAR decreases. This exact behaviour was observed in both MATLAB and COMSOL Multiphysics simulations. The dark-coloured middle part of the patient model indicates the smallest value of power absorbed by the tissue and thus low to no heating, which is the desired setup for the treatment of deep-seated tumors in the pelvic region by hyperthermia. Moreover, in both software it is possible to observe regions with elevated SAR on the opposite side of the model from the active source. This is due to the constructive interference of surface waves that travel along the surface of the water bolus and meet on the opposite side of the antenna with the same phase. These surface hotspots are inevitable in cancer treatment by hyperthermia, and HTP aims to minimise their influence on the efficiency of the treatment and effect on the patient. Luckily, the effect of surface hotspots present in the described simulations can be easily minimised by means of water bolus cooling.

To achieve agreement between the outputs from the two software, it was necessary to decrease the spatial step to $\lambda/150$. A general recommendation for accurate FDTD simulations is to have the spatial step $< \lambda/20$. It was needed to decrease the spatial step even more because of otherwise coarse, staircase-like representation of the ellipses. Decreasing the spatial step increases the simulation time. On the one hand, this kind of simulations are performed much faster in COMSOL than in MATLAB (Intel(R) Core(TM) i7-8650 CPU with a base speed of 2.11 GHz performs the simulation in COMSOL in 15 seconds while in MATLAB the process takes 343.9 seconds). On the other hand, when we start to use anatomically realistic models of the human pelvis, it will be impossible to use COMSOL Multiphysics alone, therefore, additional software is required.

6.2 Analysis of performance of the 2D FDTD-based simulator on anatomically and dielectrically realistic model of pelvic area

After successful development and implementation of the simplified simulator, its performance was tested on an anatomically and dielectrically realistic model of human pelvis. The fact that the patient model was created via the use of the Zubal numerical phantom which, in turn, is based on CT scans of a real patient, proves that this model is truly anatomically realistic. Speaking about the electric field distribution, one can see that in MATLAB the results obtained from the anthropomorphic model correspond to the expectations. Namely, it is visible that the highest amplitude of electric field is at the position of the source, and it decreases in both directions inside the patient and away from him. By referring to the provided color scale, it

is evident that the amplitude of the electric field decreases faster when the waves are propagating inside the patient. This is connected to the fact that the patient model includes many tissues, each of which has different dielectric properties, thus providing its own degree of attenuation. On the outside, however, there are only two propagating media - water and air, which do not attenuate the waves as much as biological tissues. As in the case with the simplified patient model, it is possible to see that the E-field is propagating along the geometry of the water bolus.

Speaking about comparison of FDTD-based simulator and results obtained from COMSOL Multiphysics, it is possible to conclude that both software show comparable results which proves the validity of the developed numerical simulator. From figures 5.5 and 5.6 it is evident that the highest amplitude of the E-field is in both cases at the location of the source and decreases gradually as the wave propagates through the computational domain. In both MATLAB and COMSOL Multiphysics there are regions with increased amplitude of the E-field on the surface of the water bolus, as well as on the opposite side from the location of the source. These regions arise due to constructive interference of the waves that meet with the same phase during their propagation.

Another parameter of interest was the SAR and its distribution in the model. In both MATLAB and COMSOL Multiphysics simulations there is an area with increased value of SAR in the skin region below and on the opposite side from the antenna. Hotspots in the skin region are inevitable, since skin and muscle tissue below the antenna are the first structures in the body that are exposed to the radiated RF energy. Besides, muscle tissue has relatively high electrical conductivity when compared to other biological tissues present in the simulation, thus it is considered normal that it absorbs a significant portion of the power radiated from the source. Beam steering strategies, four of which were tested in this thesis, are designed to specifically and effectively eliminate or minimise the effects of such hotspots as an addition to cooling of the body surface by the water bolus.

The high degree of similarity between the results obtained from the FDTD-based simulator and COMSOL Multiphysics for both simplified and anatomically and dielectrically realistic patient models let conclude that even for the cases of using complex geometries of the human pelvis, FDTD can be considered an accurate method as regards numerical simulations involved in HTP.

6.3 Analysis of performance of all steering strategies and evaluation of treatment planning quality

The first implemented beam steering strategy was THQ driven global optimization using PSO. The PSO optimization of the sources for one target takes on average

143.9 seconds to execute, giving the vector containing values of phases and amplitudes for each antenna at the output. This process can be accelerated via the use of special approaches, e.g. by skipping some of the spatial steps to execute calculations for a smaller number of pixels (or volume elements) or by using GPU (Graphics Processing Unit).

Speaking about qualitative evaluation of the strategy, it is possible to conclude that THQ driven global optimization is accurate and precise enough to focus the energy radiated by the sources on the area of the chosen target. By looking at figures 5.9 - 5.13 with outlined masks of targets and at their optimised SAR distributions, it is evident that the most heated region of the patient model is in the proximity of the chosen target in all 10 cases. The obtained results for all targets confirm that the main aim of the optimization by means of THQ driven algorithm was achieved - SAR within the target area was maximized while in the surrounding healthy tissue it was minimised, thus confirming that the task of maximizing the ratio of the mean SAR in the target volume and the mean SAR absorbed by the healthy tissue was successfully completed. High quality of steering without the presence of hotspots in healthy tissue other than the one present in the proximity of the tumor shows that the efficiency of the PSO is the reason why THQ driven global optimization is implemented in modern clinical practice for treating cancer. Further analysis can be performed by referring to the evaluation metrics obtained for each target - TC25 and TC50 parameters as well as best maximized THQ function values for each target.

Speaking about TC25 and TC50 parameters, from table 5.1 it stems that THQ driven global optimization steers the sources best in cases of the first and fifth targets. The first source is located in the middle of the patient model (in the position of the urinary bladder), and the fifth source is shifted down and to the (anatomical) left side from the center. In contrast to the fifth target, the value of TC25 of the fourth target, which was moved down and to the (anatomical) right side from the center of the patient model, was approximately 20 % lower. This could have occurred due to target composition - in case of the fourth target, there are less muscles and tissues constituting organs and a slightly higher amount of fat tissue, which does not absorb power as well as tissues with higher conductivity and occurs black in all presented SAR distributions. The fifth target, on the contrary, contains a higher amount of muscles which have a high value of electrical conductivity and thus greatly absorb the power radiated from the sources. In case of the second and third targets, low values of target coverage with SAR greater than 25 % or 50 % of the maximum SAR in the model are due to the bony tissues present within both these targets, which do not absorb the power and therefore lower target coverage by the energy. Other five targets are located closer to the body surface and focusing maximum energy on them causes hotspots mainly in the skin region, which is inevitable. However, this issue can be easily and effectively dealt with by water

bolus cooling. The conclusions based on the assessment of TC25 and TC50 metrics should, however, be complemented with the evaluation of the best function value of the THQ cost function. From table 5.2 it is evident that the most efficient steering was performed in cases of targets 6 and 8, as the best function value is the highest in these cases. By solely evaluating TC metrics, the heating of the healthy tissue surrounding the target contributes to higher values of this parameter, as it has been observed in cases of targets 1 and 5. In order to effectively and precisely focus the energy on the target, best function values of THQ cost function should be evaluated in conjunction with TC metrics.

The next investigated strategy was generalized eigenvalue approach. The technique is not used in modern clinical practice due to limited accuracy, however, speed and simple mathematical description are its main advantages in comparison to other beam steering strategies. Furthermore, it still might be useful in predicting the starting vector for THQ driven global optimization. In contrast to THQ driven global optimization, which takes approximately 2.5 minutes for optimizing the sources for a single target, generalized eigenvalue approach fulfils the task in a matter of 3.3 seconds. The reason for that is the absence of looping algorithms as in time reversal or iterative evaluation of best function value as in THQ driven global optimisation - only simple mathematical operations necessary for finding eigenvalues and eigenvectors of a matrix are applied, which are implemented in MATLAB in a form of a single and effective command. Nevertheless, higher degree of algorithm simplification has an inverse relation to the performance accuracy. In case of using generalized eigenvalue approach the highest value of TC25 was in case of the sixth target, which is located close to the body surface on the (anatomical) right side of the patient. In case of this steering strategy, highest values of TC25 and TC50 metrics, as well as the highest value of the THQ function correspond to the same target. This yields that the most efficient steering was indeed performed for the case of the sixth target. All targets representing deep and relatively deep-seated tumors (2, 3, 4, 5) and also target 7 have 0% coverage by the SAR that is greater than 25 % or 50 % of the maximum SAR in the model. From the four investigated algorithms, generalized eigenvalue approach is the only one that is unable to focus the SAR that would be greater than 25 % or 50 % of the maximum SAR on half of the targets.

By looking at figures 5.9 - 5.13 it is evident that in case of the first target relatively effective heating of the tumor can be achieved with minimized influence of the hotspots, whose presence on the body surface can be compensated by means of water bolus cooling. Targets 2, 3, 4, and 5 can be considered deep-seated, and while the algorithm attempts to minimise the heating of the healthy tissue surrounding the tumor, most radiated energy is absorbed by the skin and muscles close to the body surface, whereas the actual tumor receives little to no heating. In case of target 7, the algorithm failed to find a proper setting of amplitudes and phases for the antennas

and for targets 8, 9, and 10 it could effectively focus power delivery on the proper side of the patient and eliminate heating of the surrounding healthy tissue. On the whole, although the computational simplicity and speed may seem advantageous at first, it needs to be considered that generalized eigenvalue approach is not only limited to providing reasonable focusing in selected cases of surface tumors but is also not the most effective method to be used in clinical practice for effective treatment of cancer as, for example, THQ driven global optimization.

The third investigated technique was based on time-reversal. This technique is closely related to the FDTD method used for the calculation of the electric field in the model, as it uses FDTD for finding amplitudes and phases of the antennas. By looking at figure 5.9 - 5.13 one can see that this approach is suitable for steering the antennas for the cases of both surface and deep-seated tumors, however, the strategy performs better in the latter case. Speaking about TC25 parameter, in cases of targets 6, 8, and 10, all of them have 0% coverage by SAR that is greater than 25 % or 50 % of the maximum SAR. In case of TC50 all these targets and also targets 7 and 9 have 0% coverage. Time-reversal is the first investigated technique within the scope of this thesis, whose highest values of TC25 and TC50 did not correspond to the same target. Namely, the greatest value of TC25 was achieved for target 1 and greatest value of TC50 was related to target 2. In spite of this difference, it does not change the main conclusions made regarding this algorithm. Targets 1 and 2 are located relatively close to each other with the second target being slightly above the first. As can be seen from figure 5.9, if one considers actual target locations, it becomes visible that such steering better suffices for target 2, which is also manifested by a higher value of TC50. Although volume of target 1 contains more highly electrically conductive tissues which strongly absorb the radiated power from the sources, target 2 is closer to the body surface and contains more fat tissue, and due to highly conductive skin and muscles in the proximity of and within the target, the accumulated energy results in heating the target region more than in case of target 1 while the fat absorbs no power. Since the amount of biological tissues able to absorb this power is smaller in case of target 2, a surface hotspot appears and results in a higher value of TC50. This assumption is confirmed by referring to table 5.2, from which it is evident that the highest value of the THQ is in case of the second target. All in all, from the cases of 10 investigated targets it can be concluded that time reversal works better for treating tumors that are located deep in the pelvis and have enough of good or highly electrically conductive tissues around (e.g. muscles). This conclusion is supported by higher values of THQ for the cases of deep-seated rather than surface tumors in table 5.2. Despite attractive and intuitively-clear concept of using time-reversal, this technique has certain limitations which lower its performance in comparison to THQ driven global optimization. Namely, time-reversal does not consider the electrical conductivities of the tissues

when the wave is propagating from the virtual source in the center of the target to the antennas. This means that the propagation medium is considered lossless, and this significantly influences the character of the wave reaching the sources, upon which the optimization is based. In particular, in both lossy and lossless media the highest amplitude of the wave is at the location of the source while the propagation characteristics differ greatly. In a lossy medium, tissues with different electrical conductivities alter and decrease the amplitude of the wave and the wavelength, as well as change the phase shift, whereas in a lossless medium the decrease in amplitude is present as well, however, it is uniform in all directions of propagation. The same relates to the phase shift - in a lossless medium all waves propagate through the environment without any attenuation by tissues and their phase shift characteristics remain unchanged in relation to one another. This aspect of using a lossless propagation medium makes the determination of amplitude and phase differences between the sources problematic during optimization. Settings of the amplitudes and phases of antennas obtained from a wave that propagates through a lossless medium may inaccurately apply to a lossy medium through which the antenna signals propagate after being time-reversed. The effects of this limitation can be observed in table 5.5. Among all steering strategies, source optimization by time-reversal shows the lowest variation in amplitude settings for all targets.

As regards the last investigated beam steering strategy, target centre point, in case of TC25 parameter the same behaviour as in THQ driven global optimisation is noticeable - highest value is related to targets 1 and 5, while for TC50 it was calculated for targets 6 and 9. The lowest result in cases of both parameters was for the case of the seventh target. In case of the first target, the algorithm steers the sources in such a way as to provide uniform heating of the tissues along with the target and effectively avoids the formation of hotspots. In cases of second and third targets it correctly focuses the energy on the chosen side of the patient, however, in an attempt to avoid hotspots around the target, it steers the antennas in a way that creates a hotspot on the front side of the patient. In cases of targets 4 and 5 the proper side of the patient is relatively uniformly heated with the presence of two surface hotspots which can be tolerated by the patient because of water bolus cooling. Targets 6 and 9, as well as 8 and 10, are located close to each other, and from figures 5.11 and 5.13 it is visible that for targets 6 and 9, the one that is located closer to the backside of the patient leads to the creation of a smaller hotspot, while in case of targets 8 and 10 the size of the hotspots created in the proximity of the targets is almost equal. The algorithm is able to equally distribute the energy between the back and front side of the patient so as to avoid extensive heating of either of them in case of the eighth target, whereas focusing the energy on target 10 causes the creation of a hotspot, where the energy is concentrated on the front side of the patient. In case of the seventh target, the same scenario as

in the first target was observed - the algorithm attempted to find such setting of the amplitudes and phases so as to focus the energy on the target and minimise the heating of the surrounding healthy tissue, and this resulted in the creation of a hotspot on the backside of the patient, while the target region and its surroundings were uniformly heated. From the conducted measurements it was concluded that TCP has an advantage of being fast because it does not involve looping algorithms or any iterative and computationally demanding calculations and steers the sources properly for both deep and surface tumors.

On the whole, after the investigation of performance of all four beam steering strategies and their treatment planning quality it can be concluded that the most accurate and effective strategy would be the THQ driven global optimisation, however, at the cost of increased computation time dependent on the number of iterations chosen for the evaluation of best cost function value. THQ driven global optimization has the highest average value of both TC25 and TC50 from all four algorithms, while its standard deviation of these parameters is slightly higher than in TCP steering, making TCP the second best choice. TCP is fast and shows reasonable qualitative and quantitative results for deep-seated and surface tumors with lowest values of standard deviation for both TC25 and TC50 parameters. Next would be generalized-eigenvalue approach, which, in spite of its mathematically appealing form, should not be considered the main option during source optimization in HTP due to its inaccuracy and limitations related to tumor location. Although it has the largest standard deviation of both TC25 and TC50 among all four algorithms, from table 5.1 it is visible that the values of both TC25 and TC50 are comparable, and for targets 1, 6, 8, 9, and 10 generalized eigenvalue approach outperforms time-reversal. In cases of targets 2-5 both TC25 and TC50 are equal to 0, however, the results obtained from time-reversal, despite being non-zero will not be used during real clinical treatment as their values are too low to provide effective treatment. The last strategy to be considered is time-reversal which, however, is limited by the lack of the concept of electrical conductivity during wave excitation at a virtual source. It has the smallest average value of both TC25 and of TC50 and third largest value of standard deviation for both evaluation metrics. Relatively good values of TC25 for targets 2-5 do not prove that time-reversal would effectively treat such tumors, since TC50 values for the same targets are remarkably lower, and in clinical practice target coverage by the highest possible percentage of the maximum SAR in the model is of main interest. Analysis of the values of THQ function confirm that the best steering strategy from the four investigated algorithms is THQ driven global optimization, followed by TCP. According to the analysis of THQ values from table 5.2 it is evident that generalized eigenvalue approach worls best for surface tumors while time-reversal outperforms it in cases of deep-seated tumors. This assumption is confirmed by joining the evaluation of THQ for both algorithms

with obtained values of TC25 and TC50 parameters. Therefore, in order to choose the better algorithm from them it is necessary to consider the evaluation metrics, SAR distribution, THQ values and target location, and the behaviour of optimized amplitudes and phases.

7   Conclusion

The main aim of this thesis was to create a two-dimensional numerical simulator of electromagnetic field in an anatomically and dielectrically realistic model of pelvic area in the MATLAB environment and use it for studying four treatment planning algorithms. Furthermore, its performance should have been similar to the real-world case as much as possible.

One of the advantages of this simulator is that it was created using a relatively simple and intuitively understandable FDTD method. Implementation of this method yielded accurate results which were in good agreement with the expectations for both simplified and anatomically and dielectrically realistic patient model. Another advantage and an accuracy indicator is the correspondence of the behaviour of the simulation with the model analysis carried out using COMSOL Multiphysics commercial software for both cases of simplified and complex patient model. We can conclude that the MATLAB simulator is accurate, and with future testing it could effectively be integrated into cancer treatment processes.

Speaking about the study of treatment planning algorithms, it has been found that out of the four investigated beam steering strategies THQ driven global optimization is the most reliable and accurate choice which explains its widespread use in modern clinical practice. Second best-performing algorithm was TCP steering that is fast and effectively focuses the energy on the tumor regardless of its position in the body. Time-reversal has shown to perform better than generalized eigenvalue approach for the selected cases of deep-seated tumors while failing in effectively focusing the energy on the targets located close to the body surface. It is, however, associated with increased computation time and inaccuracies related to zeroed electrical conductivity of the tissues in the FDTD calculations. Generalized eigenvalue approach, on the contrary, is more appealing from the practical point of view due to its mathematically attractive form and high execution speed. Low selectivity and high dependence on tumor location of both of these strategies are not present in THQ driven global optimization and TCP method.

List of literature

1. ROSER, Max; RITCHIE, Hannah. Cancer. *Our World in Data* [online]. 2015 [visited on 2021-12-19]. Available from: ⟨https://ourworldindata.org/cancer⟩.

2. *Hyperthermia Cancer Institute: The Best Cancer Treatment You've Never Heard Of* [online]. 2020 [visited on 2021-10-31]. Available from: ⟨https://smmirror. com / 2020 / 11 / hyperthermia - cancer - institute - the - best - cancer - treatment - youve-never-heard-of/⟩. Section: News.

3. *BSD-2000 3D Microwave Hyperthermia System* [online]. [N.d.] [visited on 2021-10-31]. Available from: ⟨https://www.pyrexar.com/hyperthermia/bsd-2000-3d⟩.

4. LE, Huy; NGUYEN, Minh; YAN, Wei Qi. A Web-Based Augmented Reality Approach to Instantly View and Display 4D Medical Images. In: *ACPR (2)*. 2019, pp. 691–704.

5. SULLIVAN, Dennis M. Electromagnetic simulation using the FDTD method. In: John Wiley & Sons, 2013, p. 56.

6. *Finite Element Mesh Refinement Definition and Techniques* [online]. [N.d.] [visited on 2021-10-31]. Available from: ⟨https://www.comsol.com/multiphysics/ mesh-refinement⟩.

7. SUNG, Hyuna; FERLAY, Jacques; SIEGEL, Rebecca L; LAVERSANNE, Mathieu; SOERJOMATARAM, Isabelle; JEMAL, Ahmedin; BRAY, Freddie. Global cancer statistics 2020: GLOBOCAN estimates of incidence and mortality worldwide for 36 cancers in 185 countries. *CA: a cancer journal for clinicians*. 2021, vol. 71, no. 3, pp. 209–249.

8. *What Is Cancer? - National Cancer Institute* [online]. 2007 [visited on 2021-10-28]. Available from: ⟨https://www.cancer.gov/about-cancer/understanding/ what-is-cancer⟩. Archive Location: nciglobal,ncienterprise.

9. HOFFMAN, Matthew; MD. *The Abdomen (Human Anatomy) - Picture, Function, Parts, Definition, and More* [online]. [N.d.] [visited on 2021-10-28]. Available from: ⟨https://www.webmd.com/digestive-disorders/picture-of-the-abdomen⟩.

10. HARRINGTON Rebecca, Skye Gould. *These are the 5 deadliest cancers* [online]. [N.d.] [visited on 2021-10-28]. Available from: ⟨https://www.businessinsider. com/deadliest-worst-cancers-2016-1⟩.

11. *Types of Cancer Treatment - National Cancer Institute* [online]. 2017 [visited on 2021-10-28]. Available from: ⟨https://www.cancer.gov/about-cancer/ treatment/types⟩. Archive Location: nciglobal,ncienterprise.

12. *Radiation vs. Chemo: Uses, Benefits, Side Effects, More* [online]. 2020 [visited on 2021-10-31]. Available from: ⟨https://www.healthline.com/health/radiation-vs-chemo⟩.

13. VAN DER ZEE, Jill. Heating the patient: a promising approach? *Annals of oncology*. 2002, vol. 13, no. 8, pp. 1173–1184.

14. VANDERWAAL, R. P.; ROTI, J. L. Roti. Heat induced 'masking' of redox sensitive component(s) of the DNA-nuclear matrix anchoring complex. *International Journal of Hyperthermia* [online]. 2004, vol. 20, no. 2, pp. 234–239 [visited on 2021-10-31]. ISSN 0265-6736, ISSN 1464-5157. Available from DOI: ⟨10.1080/02656730310001627704⟩.

15. *Microwave hyperthermia for cancer treatment — Chalmers* [online]. [N.d.] [visited on 2021-10-31]. Available from: ⟨https://www.chalmers.se/en/projects/Pages/Mikrov%C3%A5gshypertermi-f%C3%B6r-cancerbehandling.aspx⟩.

16. GREEF, Martijn de. *Loco-regional hyperthermia treatment planning: optimisation under uncertainty*. S.l]; Amsterdam: s.n.] ; Universiteit van Amsterdam [Host, 2012. ISBN 978-90-8891-374-7. OCLC: 928158469.

17. BEN-YOSEF, R; KAPP, DS. Direct clinical comparison of ultrasound and radiative electromagnetic hyperthermia applicators in the same tumours. *International journal of hyperthermia*. 1995, vol. 11, no. 1, pp. 1–10.

18. DEWHIRST, Mark W; VUJASKOVIC, Zeljko; JONES, Ellen; THRALL, Donald. Re-setting the biologic rationale for thermal therapy. *International Journal of Hyperthermia*. 2005, vol. 21, no. 8, pp. 779–790.

19. OVERGAARD, Jens; HORSMAN, Michael R. Modification of hypoxia-induced radioresistance in tumors by the use of oxygen and sensitizers. In: *Seminars in radiation oncology*. 1996, vol. 6, pp. 10–21. No. 1.

20. CHICHEŁ, Adam; SKOWRONEK, Janusz; KUBASZEWSKA, Magda; KANIKOWSKI, Marek. Hyperthermia–description of a method and a review of clinical applications. *Reports of Practical Oncology & Radiotherapy*. 2007, vol. 12, no. 5, pp. 267–275.

21. JORDAN, Andreas; WUST, P; FÄHLIN, H; JOHN, W; HINZ, A; FELIX, R. Inductive heating of ferrimagnetic particles and magnetic fluids: physical evaluation of their potential for hyperthermia. *International journal of hyperthermia*. 1993, vol. 9, no. 1, pp. 51–68.

22. XIAOPING, Li; LEIZHEN, Zheng. Advances of high intensity focused ultrasound (HIFU) for pancreatic cancer. *International Journal of Hyperthermia*. 2013, vol. 29, no. 7, pp. 678–682.

23. STAUFFER, Paul R. Evolving technology for thermal therapy of cancer. *International Journal of Hyperthermia*. 2005, vol. 21, no. 8, pp. 731–744.

24. ZEE, Jacoba van der; GONZÁLEZ, Dionisio; RHOON, Gerard C van; DIJK, Jan DP van; PUTTEN, Wim LJ van; HART, Augustinus AM, et al. Comparison of radiotherapy alone with radiotherapy plus hyperthermia in locally advanced pelvic tumours: a prospective, randomised, multicentre trial. *The Lancet*. 2000, vol. 355, no. 9210, pp. 1119–1125.

25. PAULIDES, Margarethus. *Development of a Clinical Head and Neck Hyperthermia Applicator*. 2007. PhD thesis.

26. TOGNI, Paolo; VRBA, Jan; VANNUCCI, Luca. Water bolus influence on temperature distribution of applicator for small melanoma tumors. In: *2009 European Microwave Conference (EuMC)*. 2009, pp. 874–877.

27. EBRAHIMI-GANJEH, Mohammad Ali; ATTARI, Amir Reza. STUDY OF WATER BOLUS EFFECT ON SAR PENETRATION DEPTH AND EFFECTIVE FIELD SIZE FOR LOCAL HYPERTHERMIA. *Progress In Electromagnetics Research B* [online]. 2008, vol. 4, pp. 273–283 [visited on 2021-10-31]. ISSN 1937-6472. Available from DOI: ⟨10.2528/PIERB08011403⟩.

28. BULL, JOAN M; LEES, DAVID; SCHUETTE, WILLIAM; WHANG-PENG, JACQUELINE; SMITH, ROSALIE; BYNUM, GAITHER; ATKINSON, E RONALD; GOTTDIENER, JOHN S; GRALNICK, HARVEY R; SHAWKER, THOMAS H, et al. Whole body hyperthermia: a phase-l trial of a potential adjuvant to chemotherapy. *Annals of internal medicine*. 1979, vol. 90, no. 3, pp. 317–323.

29. FANI, F.; SCHENA, E.; SACCOMANDI, P.; SILVESTRI, S. CT-based thermometry: An overview. *International Journal of Hyperthermia* [online]. 2014, vol. 30, no. 4, pp. 219–227 [visited on 2021-10-31]. ISSN 0265-6736, ISSN 1464-5157. Available from DOI: ⟨10.3109/02656736.2014.922221⟩.

30. KOK, HP; WUST, P; STAUFFER, Paul R; BARDATI, F; VAN RHOON, GC; CREZEE, J. Current state of the art of regional hyperthermia treatment planning: a review. *Radiation Oncology*. 2015, vol. 10, no. 1, pp. 1–14.

31. SULLIVAN, Dennis M. Electromagnetic simulation using the FDTD method. In: John Wiley & Sons, 2013, pp. 1–3.

32. HAND, JW. Modelling the interaction of electromagnetic fields (10 MHz–10 GHz) with the human body: methods and applications. *Physics in Medicine & Biology*. 2008, vol. 53, no. 16, R243.

33. LAKHSSASSI, Ahmed; KENGNE, Emmanuel; SEMMAOUI, Hicham. Modifed Pennes' equation modelling bio-heat transfer in living tissues: Analytical and numerical analysis. *Natural Science*. 2010, vol. 02. Available from DOI: ⟨10.4236/ns.2010.212168⟩.

34. *MATLAB - MathWorks* [online]. [N.d.] [visited on 2022-04-24]. Available from: ⟨https://www.mathworks.com/products/matlab.html⟩.

35. *COMSOL: Multiphysics Software for Optimizing Designs* [online]. [N.d.] [visited on 2022-04-24]. Available from: ⟨https://www.comsol.com/⟩.

36. SULLIVAN, Dennis M. Electromagnetic simulation using the FDTD method. In: John Wiley & Sons, 2013, p. 49.

37. SULLIVAN, Dennis M. Electromagnetic simulation using the FDTD method. In: John Wiley & Sons, 2013, pp. 67–69.

38. ZUBAL, I. George; HARRELL, Charles R.; SMITH, Eileen O.; RATTNER, Zachary; GINDI, Gene; HOFFER, Paul B. Computerized three-dimensional segmented human anatomy. *Medical Physics* [online]. 1994, vol. 21, no. 2, pp. 299–302 [visited on 2021-12-24]. ISSN 2473-4209. Available from DOI: ⟨10.1118/1.597290⟩. _eprint: https://onlinelibrary.wiley.com/doi/pdf/10.1118/1.597290.

39. COLE, Kenneth S.; COLE, Robert H. Dispersion and Absorption in Dielectrics I. Alternating Current Characteristics. *The Journal of Chemical Physics* [online]. 1941, vol. 9, no. 4, pp. 341–351 [visited on 2022-01-08]. ISSN 0021-9606. Available from DOI: ⟨10.1063/1.1750906⟩. Publisher: American Institute of Physics.

40. FOUNDATION, IT'IS. *Tissue Properties Database V4.0* [online]. IT'IS Foundation, 2018 [visited on 2021-12-24]. Available from DOI: ⟨10.13099/VIP21000-04-0⟩. Medium: .h5, .xml, .txt Type: dataset.

41. *Urinary Bladder Function, Location and Pictures in Males and Females* [online]. [N.d.] [visited on 2021-12-25]. Available from: ⟨https://www.organsofthebody.com/bladder/⟩.

42. *CorelDRAW Graphics Suite — Free Trial* [online]. [N.d.] [visited on 2022-04-24]. Available from: ⟨https://www.coreldraw.com/cz/⟩.

43. BELLIZZI, Gennaro G.; DRIZDAL, Tomas; RHOON, Gerard C. van; CROCCO, Lorenzo; ISERNIA, Tommaso; PAULIDES, Margarethus M. Predictive value of SAR based quality indicators for head and neck hyperthermia treatment quality. *International Journal of Hyperthermia* [online]. 2019, vol. 36, no. 1, pp. 455–464 [visited on 2022-05-07]. ISSN 0265-6736. Available from DOI: ⟨10.1080/02656736.2019.1590652⟩. Publisher: Taylor & Francis _eprint: https://doi.org/10.1080/026567

44. KÖHLER, Torsten; MAASS, Peter; WUST, Peter; SEEBASS, Martin. A fast algorithm to find optimal controls of multiantenna applicators in regional hyperthermia. *Physics in Medicine and Biology* [online]. 2001, vol. 46, no. 9, pp. 2503–2514 [visited on 2022-05-11]. ISSN 0031-9155. Available from DOI: ⟨10.1088/0031-9155/46/9/318⟩. Publisher: IOP Publishing.

45. TREFNÁ, Hana Dobšíček; VRBA, Jan; PERSSON, Mikael. Time-reversal focusing in microwave hyperthermia for deep-seated tumors. *Physics in Medicine and Biology* [online]. 2010, vol. 55, no. 8, pp. 2167–2185 [visited on 2022-04-16]. ISSN 0031-9155. Available from DOI: ⟨10.1088/0031-9155/55/8/004⟩. Publisher: IOP Publishing.

46. PAULIDES, M. M.; BAKKER, J. F.; NEUFELD, E.; ZEE, J. van der; JANSEN, P. P.; LEVENDAG, P. C.; RHOON, G. C. van. The HYPERcollar: A novel applicator for hyperthermia in the head and neck. *International Journal of Hyperthermia* [online]. 2007, vol. 23, no. 7, pp. 567–576 [visited on 2022-05-07]. ISSN 0265-6736. Available from DOI: ⟨10.1080/02656730701670478⟩. Publisher: Taylor & Francis _eprint: https://doi.org/10.1080/02656730701670478.

Appendix A: Content of the attached ZIP file

- 17ABBBP_491299_Ksenia_Kulakova.zip

    - COMSOL Multiphysics

        * 2D_elliptical.mph
        * 2D_Zubal_Model_Complete_ver_for_field_and_SAR_export2.mph
        * 2D_Zubal_TCP

    - MATLAB

        * Ez_phasor_1.mat
        * Ez_phasor_2.mat
        * Ez_phasor_3.mat
        * Ez_phasor_4.mat
        * FDTD_2D_phasors_elliptical.m
        * fdtd_and_cole_cole_new.m
        * elliptical_export.m
        * Export_of_fields_Zubal.m
        * read_Efield_LiveLink_domain.m
        * matrix_from_vector.m
        * Optimisation_THQ.m
        * criterial_function_THQ.m
        * Optimisation_Generalized_Eigen_Value_Approach.m
        * Time_Reversal_Master.m
        * TCP_including_phase_calculation.m
        * Zubal_import.m
        * zubal_liver.mat
        * index.mat
        * rho.mat
        * sigma.mat
        * targets.m